

**UCSF**

**UC San Francisco Electronic Theses and Dissertations**

**Title**

Prefrontal Cortical Modulation of Motor and Non-Motor Functions in Parkinson's Disease

**Permalink**

<https://escholarship.org/uc/item/2wp867qm>

**Author**

Chen, Witney

**Publication Date**

2020

Peer reviewed|Thesis/dissertation

Prefrontal Cortical Modulation of Motor and Non-Motor Functions in Parkinson's Disease

by  
Witney Chen

DISSERTATION

Submitted in partial satisfaction of the requirements for degree of  
DOCTOR OF PHILOSOPHY

in

Neuroscience

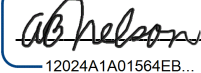
in the

GRADUATE DIVISION  
of the

UNIVERSITY OF CALIFORNIA, SAN FRANCISCO

Approved:

DocuSigned by:

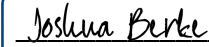


12024A1A01564EB...

Alexandra Nelson

Chair

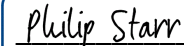
DocuSigned by:



DocuSigned by:



DocuSigned by:



ADB44FC349C54C9...

Joshua Berke

Andrew Kayser

Philip Starr

Committee Members

Copyright 2020

by

Witney Chen

## ACKNOWLEDGEMENTS

I am grateful to my PhD advisor Dr. Philip Starr for his mentorship. I thank him for taking me under his wing as his first graduate student, and for providing the time and resources to guide my growth as a scientist. I thank Phil for his empathy and compassion and for valuing my wellbeing above all.

I was fortunate to be surrounded by supportive laboratory members, both past and present, including: Coralie de Hemptinne, Nicole Swann, Andrew Miller, Doris Wang, Simon Little, and Ro'ee Gilron. I owe special thanks to Cora, who has provided guidance from the initial conception of my work to the finish line.

I thank my thesis committee, Drs. Joshua Berke, Andrew Kayser, and Alexandra Nelson, for their insights on this project.

This work would not be possible without our patients, whose selflessness expands the frontiers of human neuroscience. I also thank the clinical team members of the Movement Disorders and Neuromodulation Center for integrating basic science with their clinical duties.

I thank my family and friends who have provided emotional support beyond the laboratory to keep me sane throughout this journey. I especially thank my parents who have supported my academic pursuits—in breadth and depth—despite never having had the opportunity to seek an education themselves.



## CONTRIBUTIONS

A portion of this dissertation is a reproduction of my published material from: Chen W., de Hemptinne C., Leibbrand M., Miller A.M., Larson P.S., and Starr P.A. (2019). Altered prefrontal theta and gamma activity during an emotional face processing task in Parkinson disease. *Journal of Cognitive Neuroscience* 31:11, 1768-1776.

## **ABSTRACT**

### Prefrontal Cortical Modulation of Motor and Non-Motor Functions in Parkinson's Disease

Witney Chen

The prefrontal cortex is involved in various cognitive and affective functions. In neuropsychiatric conditions in which these functions are perturbed, such as Parkinson's disease, prefrontal activity is not well characterized, in part due to methodological constraints that limit the ability to assess neural activity with high spatial and temporal resolution in humans. We utilized high resolution invasive neurophysiology in Parkinson's patients undergoing awake, deep brain stimulation surgery to study the prefrontal cortex in Parkinson's disease.

In Chapter 1, we introduce Parkinson's disease and circuit models of disease informed by invasive recordings. Next, we discuss two studies in which we used invasive recordings to characterize prefrontal activity during movement inhibition and during emotional face processing. In Chapter 2, we introduce evidence of a prefrontal hyperdirect pathway in humans, and we characterize its topography. We found broad prefrontal innervation, with a preferential localization of fast fibers in the inferior frontal cortex. We also show inferior frontal-subthalamic co-modulation during movement inhibition, providing evidence for human hyperdirect involvement in stopping. Finally, we discuss an exploratory study of prefrontal activity during emotional face processing, where we found that Parkinson's disease is characterized by prefrontal hyperactivity (Chapter 3). These two studies expand our understanding of the prefrontal mechanisms of cognitive and affective functions in Parkinson's disease.

## TABLE OF CONTENTS

<b>Chapter 1. Introduction</b> .....	1
<b>Chapter 2. Hyperdirect Modulation of Movement Inhibition</b> .....	6
Abstract.....	6
Introduction .....	7
Methods .....	9
Results .....	15
Discussion.....	37
<b>Chapter 3. Prefrontal Activity During Emotional Face Processing</b> .....	42
Abstract.....	42
Introduction .....	43
Methods .....	45
Results .....	50
Discussion.....	57
<b>Chapter 4. Conclusions</b> .....	62
<b>References</b> .....	63

## LIST OF FIGURES

<b>Figure 2.1</b> .....	19
A fast cortical potential evoked by STN stimulation demonstrates retrograde hyperdirect activation (example from a single subject)	
<b>Figure 2.2</b> .....	20
Control experiments for evoked potentials	
<b>Figure 2.3</b> .....	22
Prefrontal cortical evoked potentials across all subjects show topography of the hyperdirect pathway	
<b>Figure 2.4</b> .....	23
Cortical topography of hyperdirect evoked potentials in all subjects	
<b>Figure 2.5</b> .....	24
Comparison of evoked potentials in left and right cortex in a single subject	
<b>Figure 2.6</b> .....	25
Comparison of cortical topography for the 6 ms and 2 ms evoked potentials	
<b>Figure 2.7</b> .....	28
Stopping-related potentials in the cortex and STN are correlated and their correlation predicts stop signal reaction time	
<b>Figure 2.8</b> .....	30
Within subjects, IFG-STN activity is initiated more quickly in successful versus failed stopping	
<b>Figure 2.9</b> .....	32
Beta power is modulated during stopping, but IFG-STN beta coherence is not correlated with stopping behavior	

<b>Figure 2.10</b> .....	33
Qualitatively similar stopping-related activity in the right and left IFG.	
<b>Figure 2.11</b> .....	35
IFG-STN coherence during stopping is not related to stopping behavior	
<b>Figure 2.12</b> .....	36
Power spectra of cortico-subthalamic cross correlograms, in 1 second window around stop and go signals, reveal beta peaks (local maxima) in some subjects but not all	
<b>Figure 3.1</b> .....	47
Emotional face processing task design	
<b>Figure 3.2</b> .....	54
High-resolution ECoG in Parkinson's and essential tremor patients	
<b>Figure 3.3</b> .....	55
Disease-specific alterations in task-related theta/alpha and high gamma activity	
<b>Figure 3.4</b> .....	56
No topographic focality in task-related high gamma activity during emotional face processing	

## LIST OF TABLES

<b>Table 2.1</b> .....	16
Patient characteristics in movement inhibition study	
<b>Table 2.2</b> .....	17
Electrode locations in movement inhibition study	
<b>Table 3.1</b> .....	51
Patient characteristics in emotional face processing study	
<b>Table 3.2</b> .....	52
Electrode locations in emotional face processing study	

# CHAPTER 1

## INTRODUCTION

### *Parkinson's disease*

Parkinson's disease is a neurodegenerative disorder characterized by both motor and non-motor symptoms. Non-motor symptoms include cognitive impairment, sleep disorders, autonomic dysfunction, and psychiatric symptoms such as depression and anxiety (K. R. Chaudhuri, Healy, Schapira, & National Institute for Clinical, 2006; K. Ray Chaudhuri & Schapira, 2009). These symptoms often predate motor symptoms, comprising the prodrome period of the disease (Kalia & Lang, 2015). The cardinal motor symptoms, of which two must be present to make a clinical diagnosis, are bradykinesia, muscle rigidity, rest tremor, and postural instability (Jankovic, 2008; Kalia & Lang, 2015). Motor and non-motor phenotypes are often heterogeneous across patients (Jankovic, 2008; Kalia & Lang, 2015).

Despite phenotypic heterogeneity, Parkinson's disease is characterized by consistent pathology. Hallmark features include the loss of dopaminergic neurons in the substantia nigra pars compacta and Lewy pathology, arising from misfolding of the  $\alpha$ -synuclein protein (Kalia & Lang, 2015).

Symptomatic therapy for Parkinson's disease begins with medications. Treatment of motor symptoms involves pharmacological agents that increase dopamine release, such as levodopa, or stimulate dopamine receptors (Kalia & Lang, 2015). Management of non-motor symptoms is more variable, but may involve psychotropics (K. R. Chaudhuri et al., 2006; K. Ray Chaudhuri & Schapira, 2009). In later stages of the disease with the emergence of levodopa-induced dyskinesias, motor fluctuations, or dopamine-unresponsive symptoms, treatment options include surgical interventions such as deep brain stimulation of the subthalamic nucleus or globus pallidus interna (DeLong & Wichmann, 2015).

In spite of well characterized neuropathology, brain network abnormalities underlying parkinsonian signs and symptoms are not well understood. Circuit models of Parkinson's disease have been informed by invasive brain recordings.

### *Invasive Brain Recordings in Humans*

Field potentials are measures of extracellular voltage deflections generated by populations of neuronal elements (Pesaran et al., 2018). In humans, these potentials can be recorded using depth electrodes, subdural electrocorticography (ECoG), and scalp electroencephalography (EEG). These methods have temporal resolutions in the millisecond range, but they differ in their spatial resolution and degree of invasiveness. Depth electrodes and ECoG offer finer spatial resolution compared to EEG, but they require invasive neurosurgical placement. These methods have the capability of assessing low frequency rhythms important for inter-region communication (Fries, 2005, 2015), as well as broadband high frequency activity that assays local cortical activation at very fast time scales (Manning, Jacobs, Fried, & Kahana, 2009; Mukamel et al., 2005).

For patients with movement disorders undergoing deep brain stimulation (DBS) surgery, invasive recordings can be used to characterize cortical-basal ganglia network activity. Acute, intraoperative recordings from DBS electrodes capture local field potentials in the basal ganglia, and temporarily placed cortical ECoG electrodes capture cortical field potentials (Panov et al., 2017). These research platforms are opening new avenues for understanding brain circuits in human disease.

### *Motor Cortico-Basal Ganglia Circuits*

Invasive brain recordings have informed the "oscillatory model" of the parkinsonian hypokinetic phenotype (de Hemptinne et al., 2013; de Hemptinne et al., 2015; Hammond, Bergman, & Brown, 2007). Oscillations represent rhythmic, synchronized sub- or supra-



threshold neural activities from groups of neurons near the recording electrode (Buzsaki & Draguhn, 2004). Neural networks can oscillate across many frequency ranges from 0.5-500 Hz, and different oscillatory frequencies have been linked to different behavioral states (Csicsvari, Jamieson, Wise, & Buzsaki, 2003; Hammond et al., 2007). Neural oscillations provide one of the key mechanisms for encoding, storing, and processing information across neural circuits by biasing the probability of neuronal spiking activity (Fries, 2005; Llinas, 1988). In Parkinson's disease, the oscillatory model posits that the cardinal motor signs are related to changes in oscillatory synchronization in beta frequencies (13-30 Hz) within and between structures of the motor network.

Elevated beta synchrony in Parkinson's disease has been linked to symptom severity. Cortico-cortical beta coherence is reduced by therapeutic levodopa and subthalamic DBS (Silberstein et al., 2005) and pallidal-cortical beta coherence is reduced by pallidal DBS (Malekmohammadi et al., 2018; D. D. Wang et al., 2018). Furthermore, cross frequency interactions between beta phase and gamma amplitude appear to be elevated in the parkinsonian state. Cross frequency coupling is an important mechanism for communication within and between neuron ensembles in different brain regions, via coordinated timing of neuronal activity in connected networks (Canolty et al., 2010; Canolty & Knight, 2010). Excessive coupling may entrain neuronal firing in an inflexible pattern that limits information encoding by spatiotemporal selectivity (Litvak et al., 2011). In the parkinsonian basal ganglia, excessive beta phase coupling to the high-frequency (200-400 Hz) amplitude in the STN is modulated by dopaminergic state (Lopez-Azcarate et al., 2010). Excessive phase-amplitude coupling also exists within the motor cortex and between the motor cortex and basal ganglia (de Hemptinne et al., 2013; de Hemptinne et al., 2015), which is reversibly suppressed by DBS (de Hemptinne et al., 2015). These abnormally synchronized activities throughout the motor network may result in hypokinesia by prohibiting the natural, dynamic neural modulation required to initiate and execute fluid movements.

Importantly, field potential oscillations themselves are not necessarily pathological. In healthy subjects, cortical beta is modulated during movement (Doyle, Yarrow, & Brown, 2005; van Wijk, Beek, & Daffertshofer, 2012) and may play a role in maintaining a motor state (Engel & Fries, 2010). However, perturbations in normal oscillatory activity may produce behavioral dysfunction. Beyond canonical motor networks, oscillatory perturbances may underlie non-motor symptoms.

### *Prefrontal Cortico-Basal Ganglia Circuits*

Multi-site LFP and ECoG recordings have largely been utilized to understand motor networks, but non-motor circuits remain poorly characterized in humans. These tools can similarly be used to study non-motor circuits in order to advance our understanding of cognitive and affective functions.

Prefrontal-basal ganglia circuits are involved in a variety of cognitive and affective processes, such as decision-making, reward-based learning, and emotion regulation. Furthermore, circuit dysfunction is associated with psychiatric disease (Gunaydin & Kreitzer, 2016). However, prefrontal-basal ganglia physiology in humans is not well characterized. In this dissertation, I focus on two functions that putatively involve prefrontal circuitry: cognitive control of movement inhibition (Aron, Behrens, Smith, Frank, & Poldrack, 2007; Atsushi Nambu, Tokuno, & Takada, 2002) and the appraisal of emotional stimuli (Carr, Iacoboni, Dubeau, Mazziotta, & Lenzi, 2003; Fusar-Poli et al., 2009; Hariri, Bookheimer, & Mazziotta, 2000; Montgomery & Haxby, 2008; Phillips, Drevets, Rauch, & Lane, 2003; Rolls, 2004).

Direct brain recordings of basal ganglia LFP and ECoG potentials have greatly informed our understanding of *motor* cortico-basal ganglia network activity in Parkinson's disease. These high spatiotemporal resolution metrics of population activity have ushered in the "oscillatory hypothesis" of movement disorders, placing an emphasis on pathological oscillatory activity in

the diseased state. From these evolving models, we can expand the use of invasive recording techniques to inform non-motor domains. While evidence points to broad range of functions of the prefrontal cortex, there is a lack of characterization of prefrontal physiology in Parkinson's disease. In this thesis, we use invasive neurophysiology to characterize the role of the prefrontal cortex in modulating movement inhibition (Chapter 2) and affective processing (Chapter 3).

## CHAPTER 2

### HYPERDIRECT MODULATION OF MOVEMENT INHIBITION

#### **Abstract**

The ability to dynamically change motor outputs, such as stopping an initiated response, is an important aspect of human behavior. A hyperdirect pathway between the inferior frontal gyrus and subthalamic nucleus is hypothesized to mediate movement inhibition, but there is limited evidence for this in humans. We recorded high spatial and temporal resolution field potentials from both the inferior frontal gyrus and subthalamic nucleus in 21 subjects. Cortical potentials evoked by subthalamic stimulation revealed short latency events indicative of monosynaptic connectivity between the inferior frontal gyrus and ventral subthalamic nucleus. During a stop signal task, stopping-related potentials in the cortex preceded stopping-related activity in the subthalamic nucleus, and synchronization between these task-evoked potentials predicted the stop signal reaction time. Thus, we show that a prefrontal-subthalamic hyperdirect pathway is present in humans and mediates rapid stopping. These findings may inform therapies to treat disorders featuring perturbed movement inhibition.

## Introduction

Stopping a movement that has already been initiated is critical for motor control. Movement inhibition is thought to be mediated by a “hyperdirect” monosynaptic pathway between the inferior frontal gyrus (IFG) and subthalamic nucleus (STN) (Aron et al., 2007; Atsushi Nambu et al., 2002). In non-human primates, anterograde tracer studies demonstrate a lateral prefrontal projection to the ventral STN (Haynes & Haber, 2013). Because of methodological constraints, however, there is limited evidence in humans that a monosynaptic IFG-STN pathway exists or that hyperdirect activation is involved in stopping. Tractography studies have identified white matter tracts between the IFG and STN (Aron et al., 2007), although imaging lacks the ability to isolate pathways that are monosynaptic. Scalp electroencephalography (EEG) studies have identified short latency evoked potentials in the frontal-central cortex elicited from STN stimulation, indicating monosynaptic connectivity (Ashby et al., 2001; Baker, Montgomery, Rezai, Burgess, & Luders, 2002; Walker et al., 2012). However, EEG lacks the spatial resolution to discern whether the pathway originates in the IFG or if it is a distributed pathway across the frontal-central cortex.

Functionally, the IFG and STN are thought to be involved in stopping (Aron, Herz, Brown, Forstmann, & Zaghloul, 2016), but activity in this pathway has not yet been characterized with high spatio-temporal resolution. Initial functional imaging studies indicated that blood oxygenation in the STN region and IFG were modulated during a stop signal task. *Single-site* invasive electrophysiology studies showed that beta band (~11-30 Hz) activity in the field potentials of the STN (Alegre et al., 2013; Kuhn et al., 2004; Ray et al., 2012) and IFG (N. Swann et al., 2009; N. C. Swann et al., 2012), assessed independently, increase during successful stopping, prompting the hypothesis that synchronized oscillatory activity in these structures mediates movement inhibition.

We utilize high-resolution, invasive electrophysiology in *both* the IFG and STN to characterize prefrontal hyperdirect topography and its functional relevance during stopping. In

Parkinson's disease patients undergoing awake neurosurgery for implantation of deep brain stimulation (DBS) electrodes, we used intraoperative electrocorticography (ECoG) targeted to the IFG, and DBS electrodes targeted to the STN. We performed evoked potentials experiments to characterize monosynaptic connectivity, and we used the stop signal task to characterize stopping-related activity. We provide physiological evidence for the existence of a prefrontal-subthalamic hyperdirect pathway in humans, show that IFG and STN are tightly synchronized during stopping, and that IFG-STN synchronization predicts stop signal reaction time across subjects.

## **Methods**

### *Subjects*

Subjects with Parkinson's disease with a clinical indication for DBS surgery were recruited from the University of California San Francisco and the San Francisco Veterans Affairs Medical Center. Inclusion criteria were: diagnosis of idiopathic Parkinson's disease confirmed by movement disorders neurologists, primary rigid-akinetic motor phenotype, Unified Parkinson's Disease Rating Scale Part III score  $\geq 30$ , and motor fluctuations on versus off dopaminergic medications. Both male and female subjects were recruited. Patients were off parkinsonian medications for at least 12 hours prior to surgery. All patients consented to have a temporary ECoG strip for research purposes during their DBS surgeries. Subjects provided informed consent prior to surgery, per protocol approved by the Institutional Review Board.

### *DBS and ECoG placement*

Unilateral neural recordings were collected from each subject, with a DBS electrode targeted to the basal ganglia and ECoG electrodes targeted to the inferior frontal cortex. The ECoG strip was placed ipsilateral to the DBS electrode.

Subjects had DBS electrodes targeted to the STN, GPi, or the ventralis intermedius nucleus of the thalamus. While the STN was the primary subcortical region studied, some subjects with pallidal and thalamic electrodes were also studied for comparison. STN DBS leads contain 4 electrodes of 1.5 mm length and 1.27 mm diameter, spaced 0.5 mm apart (Medtronic Model 3389), and GPi and thalamic leads contain 4 electrodes of 1.5 mm length and 1.27 mm diameter, spaced 1.5 mm apart (Medtronic Model 3387). DBS electrodes were placed under standard surgical protocol (Starr, 2002). The intended depth of STN leads was determined by the location of the dorsal and ventral borders of STN, mapped intraoperatively by single unit microelectrode recordings (Starr, 2002). The most dorsal contact (contact 3) was placed outside

of, and immediately dorsal to, the dorsal border of the STN. Contact 2 was placed in the dorsal (motor) territory of the STN; while contacts 1 and 0 were in the ventral STN.

A temporary, high-resolution, subdural ECoG strip (Ad-tech, Racine, WI) was inserted in the cortex ipsilateral to the STN electrode, through the same 15 mm burr hole used for DBS insertion (Panov et al., 2017). The 28-contact ECoG strip consisted of 2 rows of 14 contacts. Each contact was 1.2 mm in diameter and spaced 4 mm center-to-center. The strip was targeted to one of the three regions of the IFG: pars opercularis, pars triangularis, or pars orbitalis. Stereotactic targeting was performed with preoperative MRI using surgical planning software (Medtronic Framelink v5.1, Minneapolis, MN). Neural recordings began at least 30 min after cessation of propofol, after which it does not affect neuronal activity (Herrick et al., 1997; Raz, Eimerl, Zaidel, Bergman, & Israel, 2010). No other sedatives were used during awake neural recordings.

#### *Anatomic localization of electrodes*

To anatomically localize ECoG and basal ganglia contacts, we fused intraoperative CT images with the preoperative MRI (Panov et al., 2017). The preoperative T1 MRI was used to reconstruct individual cortical surface models in FreeSurfer (Dale, Fischl, & Sereno, 1999; Fischl et al., 2002). We projected ECoG contacts on to the cortical surface mesh using the *img\_pipe* toolbox (Hamilton, Chang, Lee, & Chang, 2017) and a surface vector projection method (Kubaneck & Schalk, 2015). Individual cortical surfaces were fit to the Desikan-Killiany atlas brain to generate cortical anatomy labels for each ECoG contact (Desikan et al., 2006).

#### *Evoked potentials stimulation*

To assess hyperdirect topography in the STN, each subject received ventral and dorsal STN stimulation while ipsilateral cortical activity was recorded. Each stimulation block was 30 s in duration, using 10 Hz pulses and biphasic square waves with 100  $\mu$ s pulse width. We tested



multiple stimulation settings at each site, varying the stimulation current and electrode configuration, to ensure that evoked potentials were not artifactual. We tested stepped stimulation currents between 3 and 6 mA to see if evoked responses scaled with current. We tested stimulation paradigms that reversed the polarity of the stimulation artifact and assessed the polarity of the evoked potentials. For bipolar stimulation, we reversed the cathode/anode configuration. For monopolar stimulation, we tested two biphasic square wave designs: negative phase followed by positive phase and vice versa.

### *Stop signal task*

A visual stop signal task was programmed using PsychToolbox for MATLAB (Mathworks, Natick, MA). Subjects performed 196-288 total trials, depending on intraoperative time constraints. During GO trials (66% of all trials), subjects were presented with an arrow pointing left or right, instructing a left or right button press, respectively. Subjects performed the task with the hand ipsilateral to the recorded side, unless there was significant tremor in that hand. During STOP trials (33% of all trials), a stop cue appeared after a variable stop signal delay, and subjects were instructed to halt movement. A staircase procedure was used to adjust stop signal delays in order to achieve approximately 50% stopping success for each subject (Verbruggen et al., 2019).

### *Signal recordings*

Evoked potential experiments were conducted using the Neuro Omega system (Alpha Omega, Nazareth, Israel), which delivered stimulation through the STN channels and simultaneously recorded ECoG potentials. Custom MATLAB scripts were written to implement stimulation. The Neuro Omega signals were recorded at a 22 KHz sampling rate and 0.075-3500 Hz bandpass filtered. Neural data during the stop signal task were collected on either the Neuro Omega or TDT PZ5 (Tucker Davis Technologies, Alachua, FL). The TDT signals were

recorded at 3 kHz and 0.45-1350 Hz bandpass filtered. We recorded ECoG potentials with two different referencing schemes to rule out the contributions of the reference electrodes to the evoked potentials. All ECoG potentials were recorded referenced to either an ipsilateral scalp needle placed subcutaneously in the vertex or scalp needles placed bilaterally in the mastoids.

### *Evoked potentials analysis*

To generate the cortical responses to subthalamic stimulation, 250 of the 300 total ECoG epochs were time-locked to stimulation and averaged. The 50 trials near the onset and offset of the entire stimulation block were discarded due to potential artifacts. The evoked responses were smoothed using a moving average filter. Peaks and troughs, and their associated amplitudes, were identified using MATLAB function *findpeaks*. To normalize evoked potential amplitudes per patient, the largest amplitude evoked potential was identified per ECoG strip. All other evoked potential amplitudes across the ECoG strip were normalized as a percentage of that maximum evoked potential. We excluded ECoG electrodes with high impedances or high amplitude noise.

### *Stop signal task analysis*

Behavioral data were analyzed to ensure that the assumptions of the race model were met. Subjects were excluded when their mean unsuccessful STOP reaction times were greater than their mean successful GO reaction times (Verbruggen et al., 2019). In subjects who did not violate the race model, the stop signal reaction time was estimated by subtracting the mean stop signal delay from the mean go reaction time.

Temporal and spectral properties of the neural data were assessed during the task. To generate event-related potentials (ERPs), time series data were first low pass filtered below 250 Hz to remove high frequency intraoperative noise. Epochs of ECoG and STN potentials were time-locked to the STOP cue and averaged. To assess the similarity and time lag of cortical and

STN potentials, cross correlations were generated for the averaged ECoG and STN ERPs. Statistical analyses of cross correlations were performed using bootstrapping, with 10,000 surrogate cross-correlations time-locked to shuffled points. To verify the lag calculated using cross correlations, the temporal offset between cortical and STN ERPs were also calculated with a second method: in channel pairs where we could identify distinct matching deflections in the ERPs, we calculated the time lag between the maxima of the deflections in the cortex and the STN. Spectral properties of the cross-correlations were assessed by calculating the power spectral density using Welch's periodogram.

To generate task-related spectrograms, data were down-sampled to 1000 Hz. Frequency decomposition was performed using wavelet convolution (Canolty et al., 2007). Data were filtered with Gabor wavelets into 128 center frequencies ranging from 2.5-250 Hz. Epochs of data were time-locked to either the GO or STOP cue. We randomly sub-selected the trials for each condition to equalize the total number of trials that contributed to GO and STOP spectrograms. The epochs were averaged and each frequency in the spectrogram was baseline corrected by subtracting the average power of a 500 ms window in the preceding inter-trial interval. Spectrograms were z-score normalized with bootstrapping: we generated a surrogate distribution of task-related activity time-locked to 10,000 shuffled points. Within subjects, an average spectrogram per anatomic region was calculated by averaging all contacts within the same region. Grand averaged spectrograms were then generated by averaging across all patients. Task-related power was quantified for the following frequency ranges: delta (1-4 Hz), theta (4-8 Hz), alpha (8-13 Hz), beta (13-30 Hz), and gamma (50-150 Hz). To calculate task-related coherence, we calculated coherence per frequency range between each IFG contact and the ventral STN in each subject. We averaged coherence in all channel pairs per patient.

For analysis of patient-specific narrow band beta modulation, we first identified the channel with the maximum task-modulated beta power per patient: based on the z-scored trial-averaged spectrograms, we selected the channel with the maximum mean 13-30 Hz beta

modulation in the 500 ms window surrounding the SSRT. For this single channel per patient, we specified a patient-specific narrow band beta by identifying the maximum frequency in the peak of the power spectra, within the 13-30 Hz range. We took a 6 Hz window around that peak frequency and filtered the data in that frequency band. Beta burst thresholds were identified using the empirical method (Shin, Law, Tsutsui, Moore, & Jones, 2017). Briefly, we calculated the mean and standard deviation of the beta amplitude envelope. Bursts were identified as events that crossed a threshold, and we tested multiple threshold values, which were stepped increments of the standard deviation. We chose the threshold that yielded bursts that were most highly correlated with overall beta amplitude. We quantified beta amplitude, burst rate, burst size, and burst duration across all trials in the 250 ms window before and after the SSRT and as well as before and after the GO RT. These metrics were averaged across trials per patient.

### *Statistical analyses*

Data are represented as mean  $\pm$  standard deviation. Kolmogorov-Smirnov tests for normality were used to determine whether parametric (t-test) or non-parametric (Wilcoxon signed rank, Wilcoxon rank sum) statistical tests were used. Pearson correlation was used for correlations between two continuous variables, and Spearman correlation was used for correlations involving ordinal variables. Bootstrapping was used to identify significant task-related modulations. A p-value  $< 0.05$  (corrected for multiple comparisons where appropriate) was considered statistically significant. Statistical tests are reported in the main text.

## Results

### *Subjects*

We enrolled 21 subjects with Parkinson's disease: 16 subjects participated in the evoked potentials experiments and 15 subjects performed the stop signal task (10 subjects participated in both) (**Table 2.1, Table 2.2**). Evoked potentials data from 2 subjects were excluded due to technical failures. Stop signal task data from 5 subjects were excluded due to violation of the race model, in which unsuccessful STOP reactions times were greater than successful GO reaction times (Verbruggen et al., 2019). Subjects were off dopaminergic medications for 12 hours. The mean DBS electrode coordinates for the right STN, aligned to the anterior commissure-posterior commissure line, were  $10.7 \pm 0.6$  (lateral),  $-3.5 \pm 1.7$  (anterior-posterior),  $-6.2 \pm 1.4$  (vertical). Coordinates for the left STN were  $-11.5 \pm 0.7$ ,  $-3.4 \pm 1.1$ ,  $-7.4 \pm 1.5$ . The mean age of subjects was  $67.5 \pm 6.3$  years and mean disease duration was  $8.6 \pm 3.4$  years.

**Table 2.1.** Patient characteristics in movement inhibition study

	Age	Sex	Disease Duration (years)	UPDRS-III ON/OFF Meds	Evoked Potentials	Stop Signal Task	Dominant Hand	Task Hand
PD 159	64	M	8	23/49	X			
PD 160	61	M	10	9/33	X			
PD 162	65	M	3	21/41	X			
PD 165	59	M	10	4/44		X	R	R
PD 166	60	M	11	8/21	X	X	R	R
PD 167	66	M	7	38/46	X	X	R	R
PD 168	76	M	3	28/36		X	R	L
PD 173	59	M	10	29/46		X	R	L
PD 176	63	M	3	18/32	X	X	R	R
PD 177	57	M	10	23/44		X	R	R
PD 183 <sup>o</sup>	60	M	13	20/36	X			
PD 184	71	M	10	16/39		X	R	R
PD 186	63	M	7	30/47	X	X	R	R
PD 187	68	M	17	41/60	X	X	R	R
PD 188 <sup>*o</sup>	59	M	7	35/55	X	X	R	R
PD 189*	51	F	7	11/28	X	X	R	R
PD 193	67	M	5	21/41	X			
PD 194*	71	F	8	--/68	X	X	R	L
PD 198*	71	M	7	37/60	X	X	R	R + L
PD 199*	76	M	10	38/58	X	X	R	R
PD 200	67	M	11	25/33	X			

M = male; F = female; UPDRS-III = Unified Parkinson's Disease Rating Scale Part III; R = Right; L = Left

\* Stop signal data excluded

<sup>o</sup> Noisy data

**Table 2.2.** Electrode locations in movement inhibition study

	Recorded Hemisphere	DBS Target	Number of ECoG Contacts					
			IFG pars opercularis	IFG pars orbitalis	IFG pars triangularis	Pre-central	Rostral Middle Frontal	Superior Temporal
PD 159	R	STN	6	0	0	9	8	5
PD 160	R	STN	0	9	14	0	0	0
PD 162	L	STN	0	0	12	0	12	4
PD 165	R	STN	5	11	11	0	0	0
PD 166	R	STN	10	0	6	0	6	6
PD 167	R	STN	10	0	6	0	6	6
PD 168	L	VIM	0	10	14	0	2	0
PD 173	L	STN	8	0	5	0	11	4
PD 176	R	STN	6	0	0	9	9	3
PD 177	R	STN	0	5	17	0	6	0
PD 183	R	STN	4	0	2	5	6	8
PD 184	R	STN	16	0	0	1	3	8
PD 186	R	STN	4	0	8	2	0	12
PD 187	R	STN	2	0	6	6	8	6
PD 188	R	STN	0	4	14	0	10	0
PD 189	R	STN	0	0	4	0	6	0
PD 193	R	STN	2	0	11	0	10	5
PD 194	L	GPI	13	0	0	1	8	6
PD 198	L	STN	17	0	0	0	5	4
PD 199	R	GPI	22	0	0	0	4	2
PD 200	R	STN	11	0	2	0	5	8

R = right; L = left; STN = subthalamic nucleus; VIM = ventralis intermedius nucleus of the thalamus; GPI = globus pallidus interna

*STN stimulation evokes cortical potentials after ~2 ms*

First, we found evidence for a prefrontal-subthalamic hyperdirect pathway in humans by stimulating in the STN and examining antidromic evoked activity in the prefrontal cortex. Short latency potentials in the cortex support the existence of a fast-conducting monosynaptic connection. **Figure 2.1** illustrates evoked cortical activity in a single subject example. Contacts were localized both with imaging (**Fig 2.1a,b**) and electrophysiology (**Fig 2.1c**). Bipolar stimulation in the right STN in the two most ventral STN contacts evoked activity in the ipsilateral ECoG after ~2 ms (**Fig 2.1d**). Because the short latency evoked potential was small in amplitude, we summed the evoked potentials elicited from two stimulation settings with reversed anode and cathode configurations, similar to previous EEG studies (Walker et al., 2012). We quantified the amplitude of the 2 ms evoked potential to characterize the subthalamic and cortical topography of the hyperdirect pathway. We found that ventral STN stimulation elicited larger amplitude potentials than dorsal STN stimulation, suggesting stronger prefrontal-ventral STN connectivity ( $p=4.0 \times 10^{-6}$ , Wilcoxon signed rank; **Fig 2.1e**). Furthermore, greater evoked potential amplitudes were found in channels covering the IFG regions compared to neighboring regions, suggesting stronger hyperdirect connectivity for the IFG than more distant cortical regions (**Fig 2.1f**).



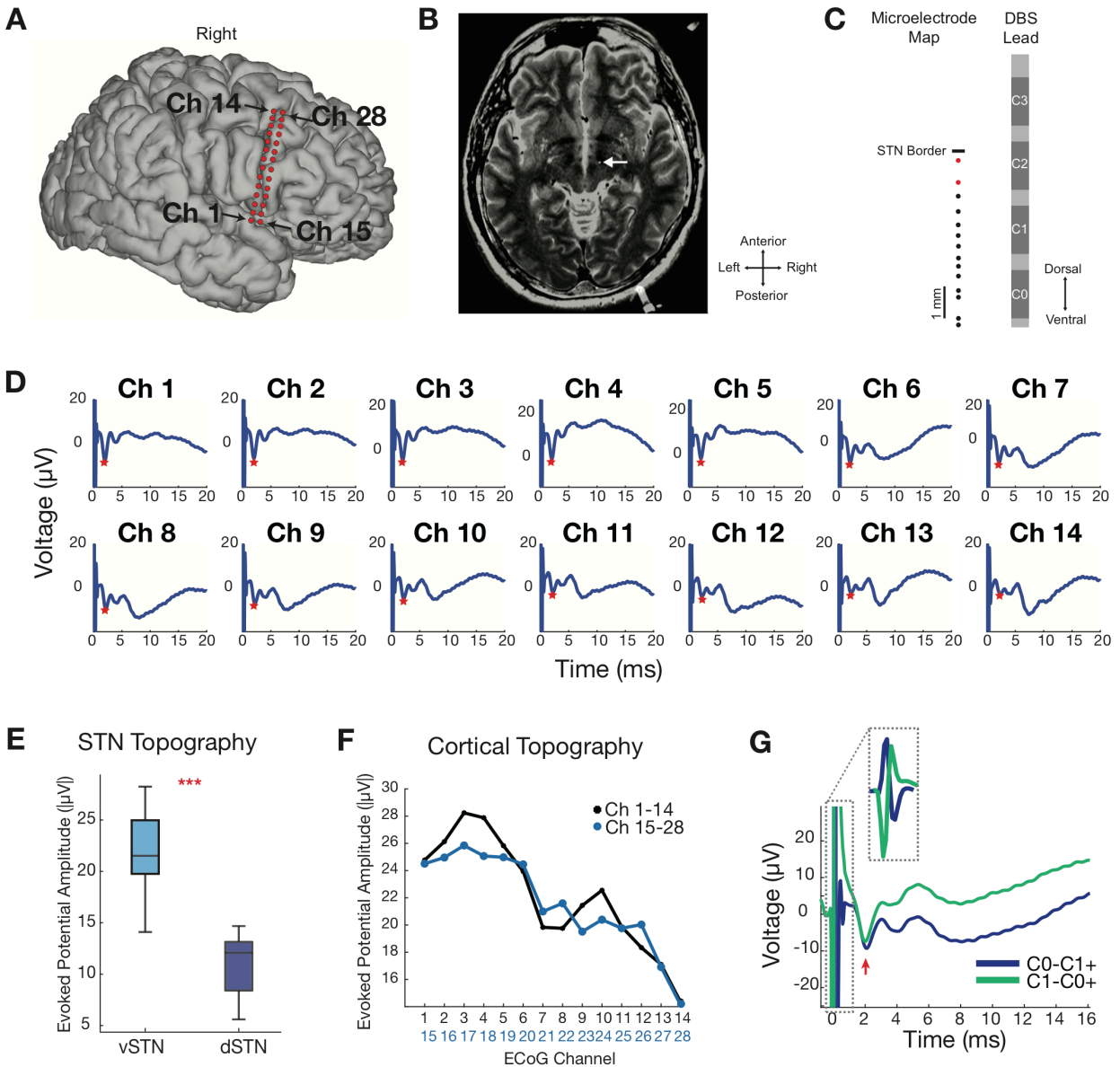


**Figure 2.1.** A fast cortical potential evoked by STN stimulation demonstrates retrograde hyperdirect activation (example from a single subject). **a)** 3D reconstruction of ECoG channel locations from intraoperative CT. **b)** DBS lead location in the STN (marked with arrow) in an axial view of the preoperative MRI fused with the intraoperative CT. **c)** Placement of DBS lead (right) according to microelectrode map (left). Single units with 20-50 Hz irregular discharge, marked with dots, are used to define the borders of the STN. Cells that responded to passive arm or leg movements (red dots) localized the dorsal (motor) STN. **d)** Cortical evoked potentials in channels 1-14 elicited from ventral subthalamic stimulation (C0-C1+, 6 mA). Earliest latency potentials occur at ~2 ms. **e)** Ventral STN stimulation elicits larger amplitude evoked potentials than dorsal STN stimulation. **f)** Cortical topography of evoked potential amplitudes in this subject. Amplitudes are higher over inferior frontal regions. **g)** Reversal of the stimulating anode and cathode reverses the polarity of the stimulation artifact, but not the polarity of the 2 ms potential (see inset), arguing against an artifactual origin of the 2 ms potential.

We ruled out artifactual contributions to this short latency, low amplitude event by manipulating stimulation and recording paradigms. Reversal of the stimulating anode and cathode reversed the stimulation artifact, but not the polarity of the evoked potential (**Fig 2.1g**). We performed additional control experiments in 5 subjects. Evoked potentials scaled with stimulation current (**Fig 2.2a**), were invariant to ECoG referencing scheme (**Fig 2.2b**), were not a cumulative effect of constant 10 Hz stimulation (**Fig 2.2c**), and did not arise from pallidal stimulation (**Fig 2.2d**).

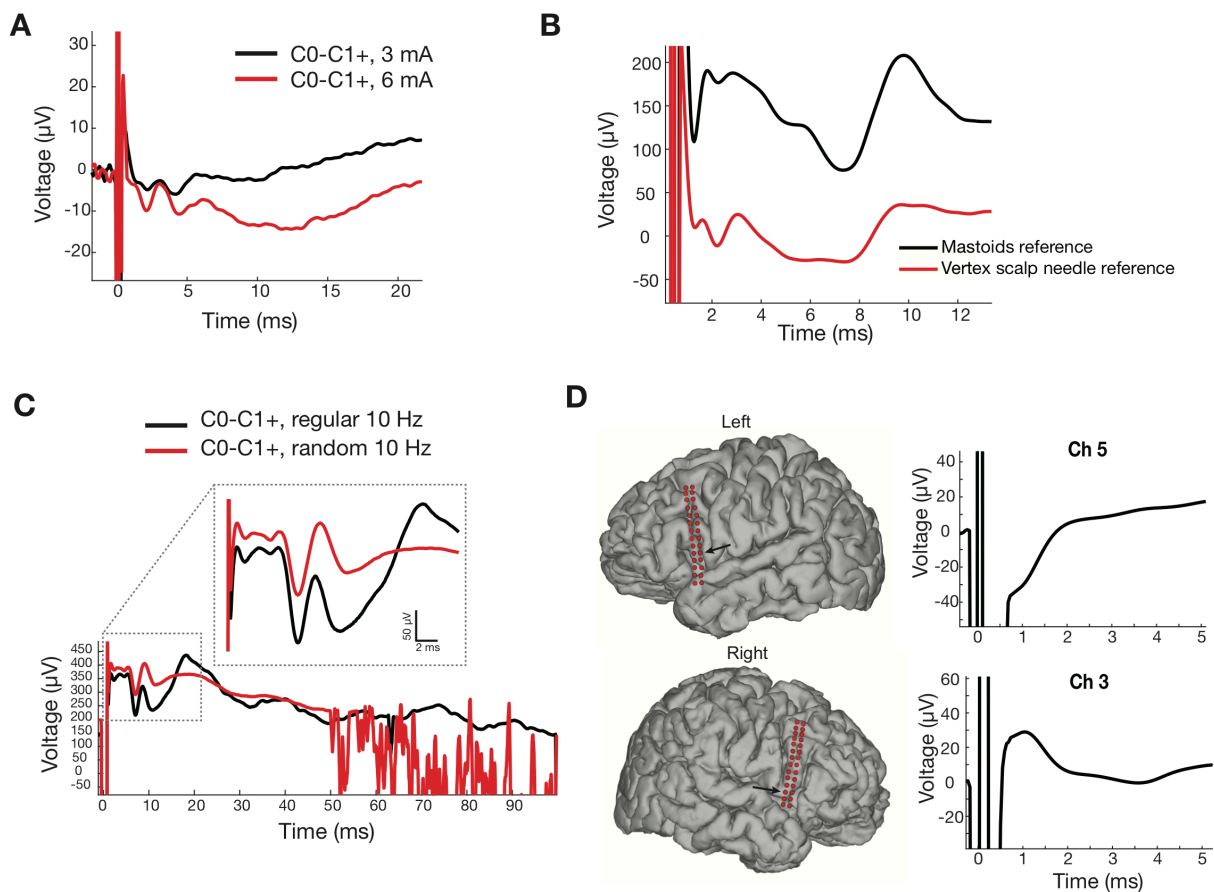


**Figure 2.2.** Control experiments for evoked potentials. **a)** Hyperdirect evoked potential amplitude scales with current amplitude. **b)** Hyperdirect evoked potential is invariant to referencing method. The potential at 2 ms is present using bilateral scalp needles in the mastoids for reference and using a scalp needle placed in the vertex. **c)** Hyperdirect evoked potential is not introduced by cumulative effects of regular 10 Hz stimulation. Regular 10 Hz stimulation and irregular stimulation that averages to 10 Hz produce similar early latency evoked potentials. **d)** Hyperdirect pathway is specific to cortex and STN. In two subjects with pallidal stimulation, there was no evoked potential at 2 ms.

Across all subjects, we conducted matched analyses of evoked potential latency, subthalamic topography, and cortical topography. The mean latency of the earliest cortical evoked potential following STN stimulation was  $2.2 \pm 0.2$  ms (**Fig 2.3a**). Ventral STN stimulation elicited larger amplitude evoked potentials than dorsal STN stimulation ( $p=4.9 \times 10^{-4}$ , Wilcoxon signed rank test; **Fig 2.3b**). In the cortical regions that we covered, evoked responses were greatest in the IFG and the perisylvian region of the superior temporal lobe, with a tapering of amplitudes in peripheral regions (**Fig 2.3c, Fig 2.4**).

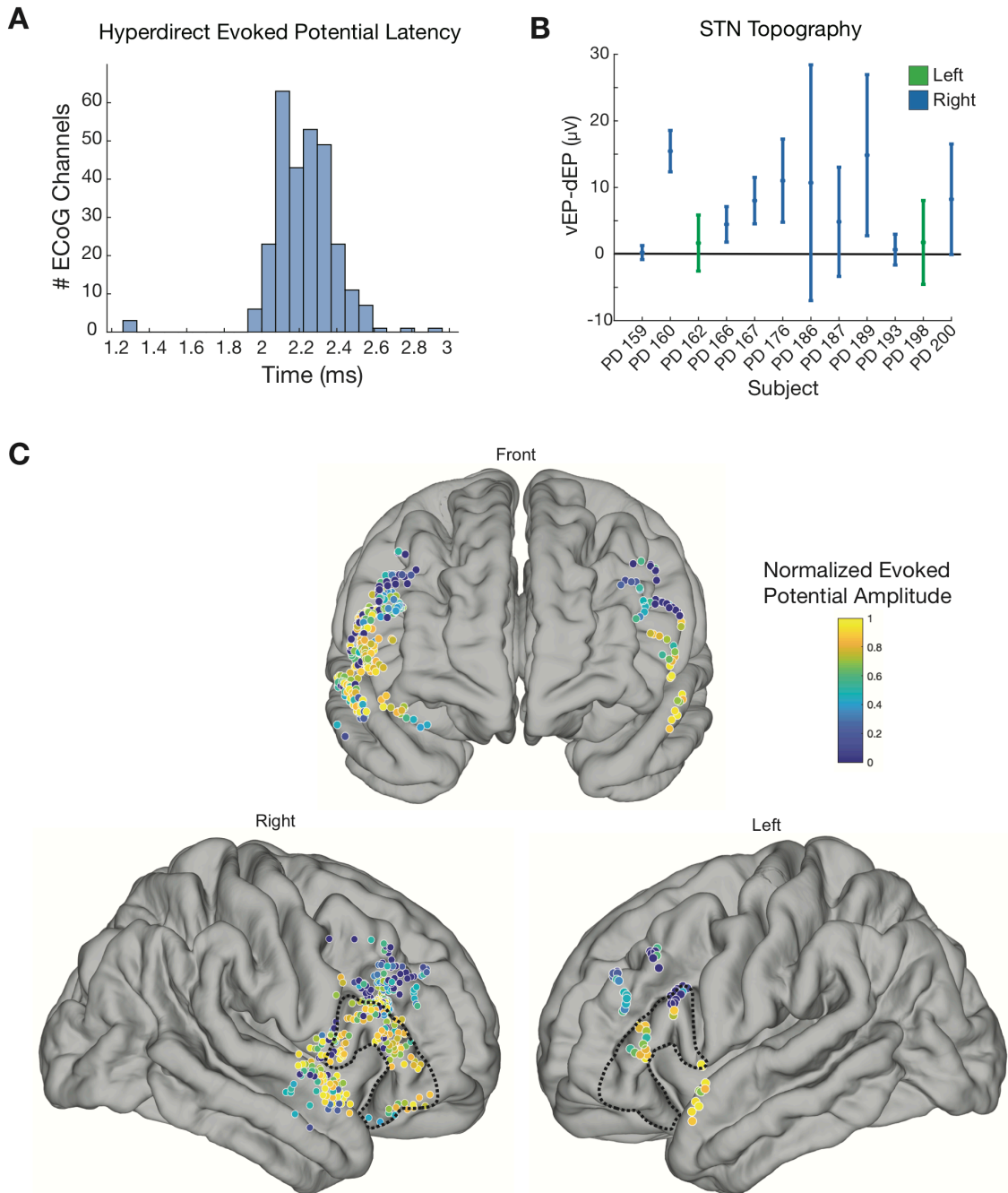


**Figure 2.3.** Prefrontal cortical evoked potentials across all subjects show topography of the hyperdirect pathway. **a)** Histogram of latencies for the earliest evoked potential across all patients (mean  $2.2 \pm 0.2$  ms). **b)** The mean and standard deviation of the difference between ventral versus dorsal evoked potential amplitudes are plotted for each subject, showing larger potentials from ventral stimulation in most subjects. **c)** Composite 3D heatmap of the normalized evoked potential amplitudes. Color indicates the EP amplitude compared to the highest amplitude recorded in the same ECoG strip. The highest amplitudes are within the IFG regions (dotted black line) or perisylvian temporal cortex in close proximity to IFG. Sulci appear larger in the atlas brain compared to an individual brain.

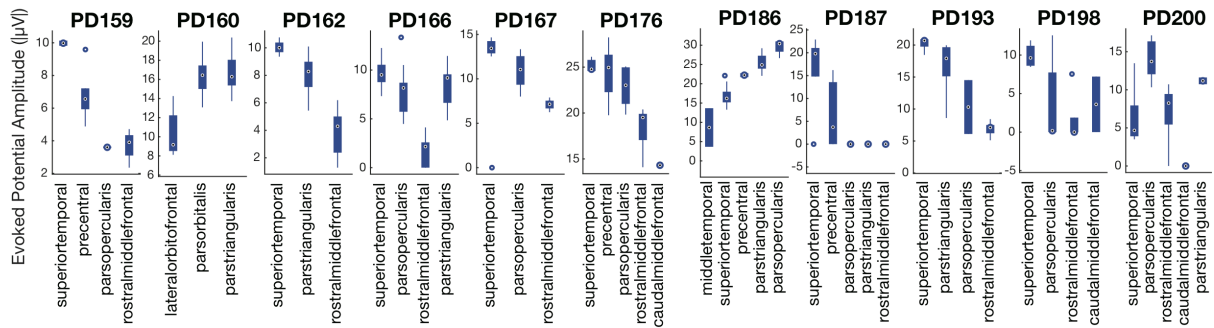


**Figure 2.4.** Cortical topography of hyperdirect evoked potentials in all subjects. Amplitude of earliest latency evoked potential per cortical region per subject.

Hyperdirect evoked potentials were elicited in the hemisphere ipsilateral to the stimulated STN, in subjects with left or right ECoG coverage. To compare evoked activity in both hemispheres, we evaluated evoked potentials in a single subject who received both left and right ECoG during two separate surgeries (**Fig 2.5a**). We found similar evoked responses ~2 ms after left and right STN stimulation, indicating that prefrontal projections to the STN are not strongly lateralized (**Fig 2.5b**). The latency of the evoked response was earlier on the right hemisphere than left ( $p=5.9 \times 10^{-4}$ , Wilcoxon rank sum; **Fig 2.5c**). Cortical topography was similar on both sides (**Fig 2.5d**), with the smallest evoked responses in contacts furthest from the IFG.

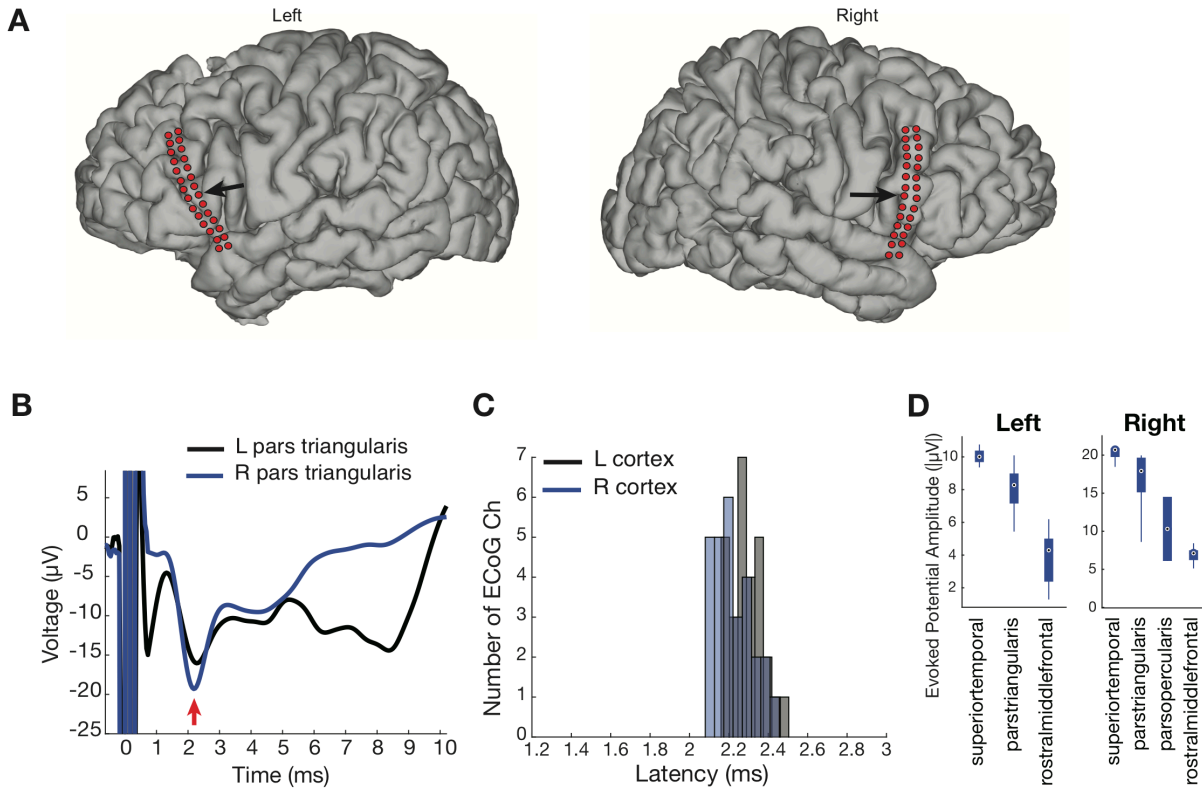


**Figure 2.5.** Comparison of evoked potentials in left and right cortex in a single subject. This subject had ECoG placed on each hemisphere during two separate surgeries for DBS implantation. **a)** 3D reconstruction of ECoG locations in the left and right hemispheres. **b)** Evoked potential traces for a single ECoG channel in left pars triangularis and right pars triangularis (marked with arrows in A). Hyperdirect potential is elicited in both hemispheres. **c)** Histogram of latencies for hyperdirect potentials in left and right cortex. **d)** Cortical topography of evoked potential amplitudes left and right hemispheres.

Following the 2 ms potential, the next distinct cortical evoked event occurred  $6.0 \pm 0.35$  ms after stimulation (**Fig 2.6a**). Even at this longer latency, conduction is still rapid enough to be mediated by retrograde activation of hyperdirect fibers, so we also assessed the topography of this longer latency potential. We found subjects in which the topography of the 6 ms potential clearly differed from that of the 2 ms potential, with larger amplitudes over dorsolateral prefrontal cortex than over the IFG, although in other subjects the topographies did not differ (examples in **Fig 2.6b**). Across all subjects, the 6 ms potential was more broadly distributed across the prefrontal cortex (**Fig 2.6c**). This suggests that a more “diffuse” hyperdirect pathway from



widespread prefrontal areas could utilize slightly smaller diameter axons, while the largest diameter, shortest latency fibers are relatively more restricted to IFG-STN pathway (**Fig 2.3c**).

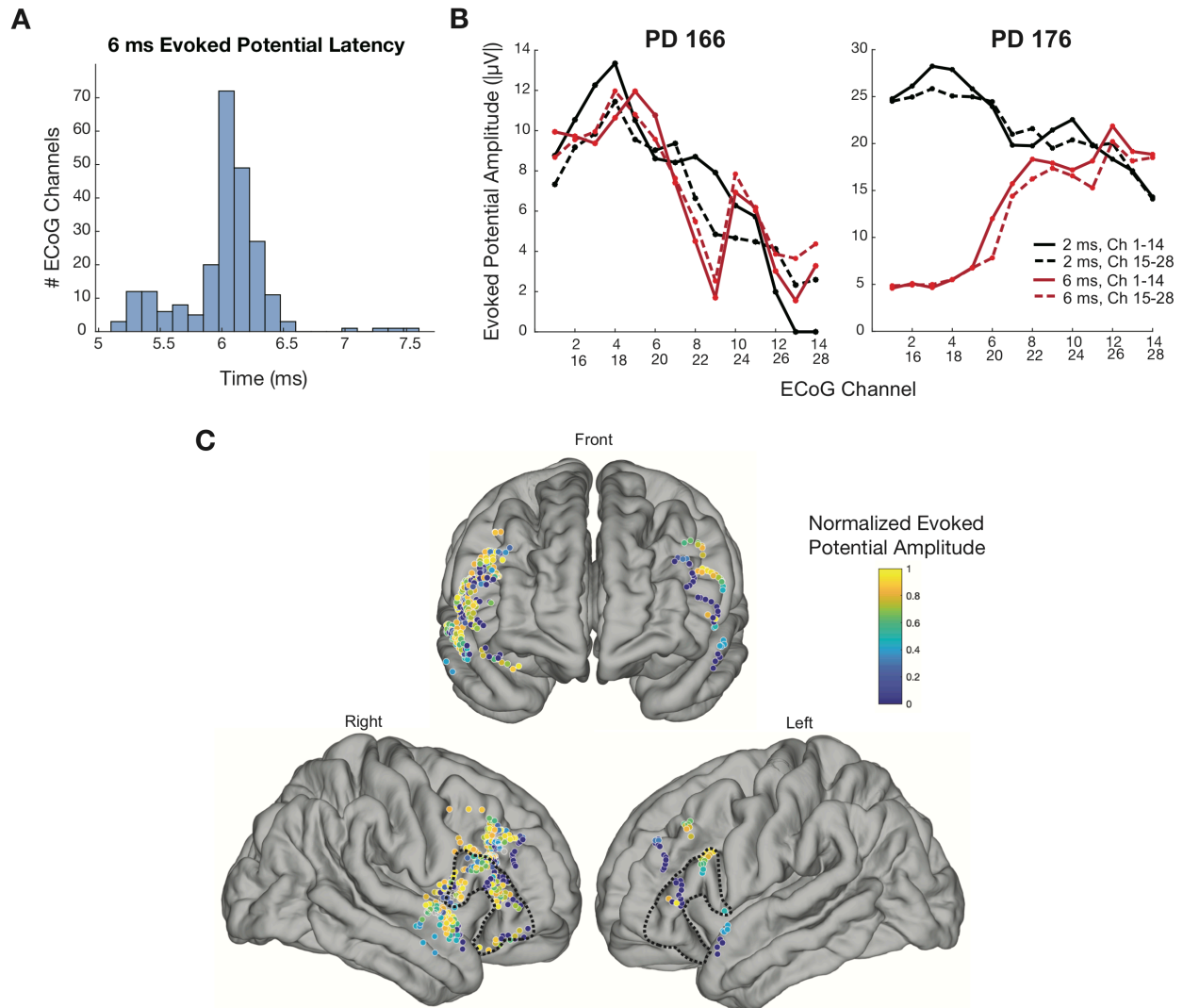


**Figure 2.6.** Comparison of cortical topography for the 6 ms and 2 ms evoked potentials. **a)** Histogram of latencies for the 6 ms evoked potential across all patients (mean  $6.0 \pm 0.35$  ms). **b)** Examples of cortical topography of the 2 ms and 6 ms evoked potentials in two subjects. In the left example, the two potentials have similar topography and in the right example, the topography differs. **c)** Composite 3D heatmap of the normalized evoked potential amplitudes for 6 ms potential for all subjects. Color indicates the EP amplitude compared to the highest amplitude recorded in the same ECoG strip, as in Figure 2.3c. Highest amplitude potentials are broadly distributed across the covered prefrontal cortical regions.

*Synchronized task-related potentials in the IFG and STN are correlated with stopping speed*

To characterize the role of the prefrontal-subthalamic hyperdirect pathway in movement inhibition, subjects performed a visual stop signal task (**Fig 2.7a**). In 66% of trials, a left or right arrow cued a left or right button press, respectively (GO trials). In 33% of trials, a stop cue followed the go cue after a variable delay, signaling a halt in movement (STOP trials). Across all subjects, mean GO trial accuracy was  $86 \pm 10\%$  and mean STOP accuracy was  $66 \pm 11\%$  (**Fig 2.7b**). Mean GO reaction time was  $779 \pm 193$  ms, mean stop signal delay was  $441 \pm 209$  ms, and estimated stop signal reaction time was  $384 \pm 76$  ms (**Fig 2.7b**).

We generated event-related potentials (ERPs) of cortical and STN evoked activity during the task. After the STOP cue in successful stop trials, ERP deflections appear in both the cortex and STN after  $\sim 200$ - $300$  ms (**Fig 2.7c**). To quantify the lag between cortical and subthalamic ERPs, we calculated the cross correlation (**Fig 2.7d**). Across subjects, the average cross correlation lag between all cortical-STN channel pairs was  $-90 \pm 131$  ms, with cortex leading the STN ( $p=0.029$ , t-test; **Fig 2.7e**). We validated our metric for prefrontal-STN lag by quantifying the temporal offset of cortical and STN ERPs with one alternative method. In ECoG and STN channels where we could identify distinct, matching ERP deflections, we calculated the difference in time between the deflection onset (maximum point in the upward deflection). Both calculations of cortico-STN ERP latency offset indicate that cortical activity precedes subthalamic activity during stopping (**Fig 2.7e**).

Next, we asked if the degree of circuit co-activation was linked to behavior. The mean prefrontal-subthalamic correlation across subjects was  $0.46 \pm 0.15$  (**Fig 2.7f**). Across subjects, the degree of correlation was inversely related to the stop signal reaction time ( $p=0.040$ ,  $r=0.65$ , Spearman correlation; **Fig 2.7g**), suggesting that greater hyperdirect circuit activity is linked to faster stopping. Although movement inhibition is impaired in Parkinson's disease (Gauggel, Rieger, & Feghoff, 2004), we did not find physiology or stopping behaviors to be correlated with



parkinsonian severity: subjects' total scores on the Unified Parkinson's Disease Rating Scale were not correlated with the stop signal reaction time ( $p=0.82$ ,  $r=0.084$ , Pearson correlation) or with cortico-STN correlation during stopping ( $p=0.72$ ,  $r=0.13$ , Pearson correlation).

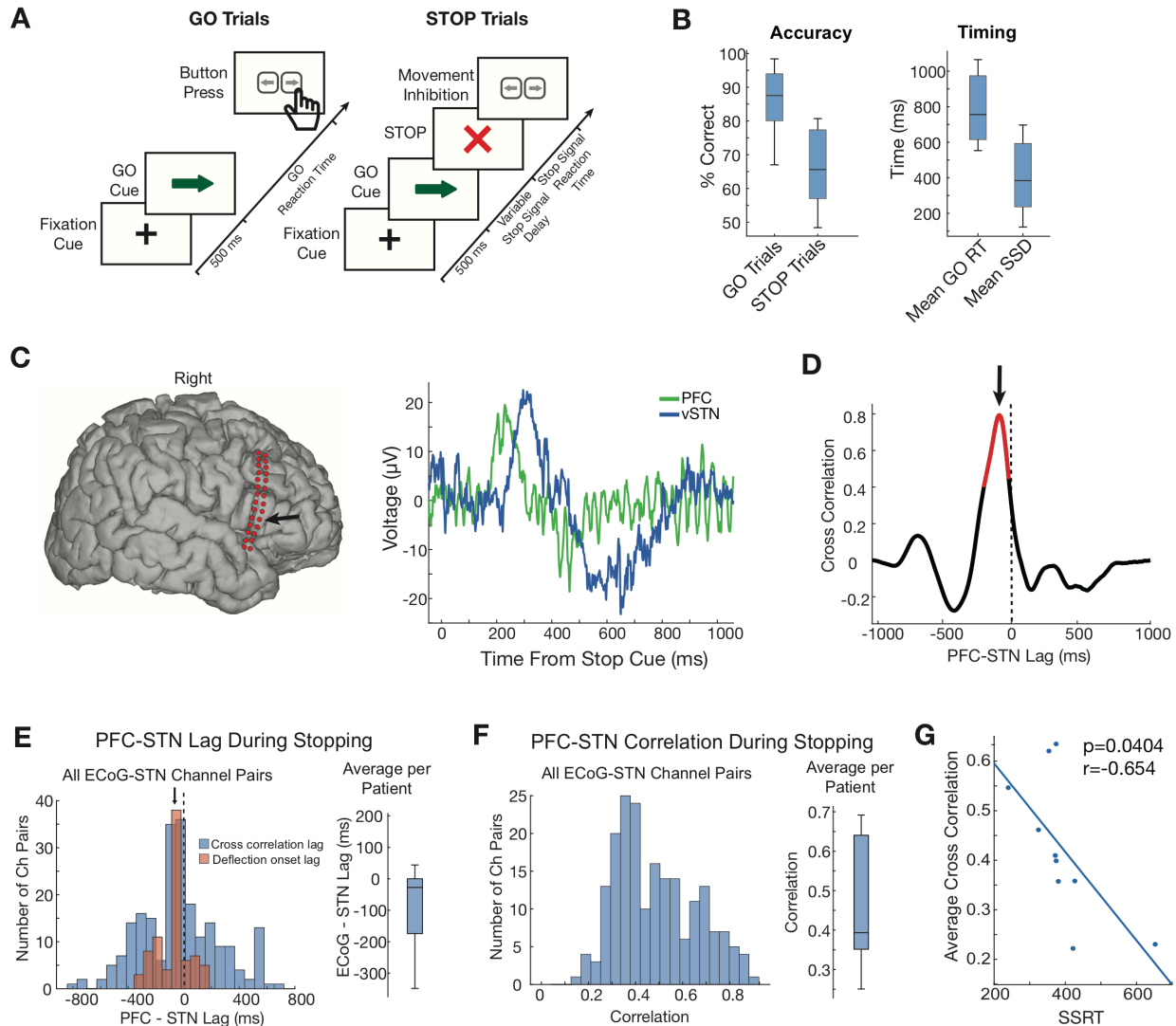


**Figure 2.7.** Stopping-related potentials in the cortex and STN are correlated and their correlation predicts stop signal reaction time. **a)** Schematic of visual stop signal task. **b)** Behavioral performance on the task. **c)** Averaged event-related potentials of 41 successful stop trials time-locked to the stop cue in a single subject. Potentials were recorded from the ventral STN and from one cortical contact (location indicated with arrow on the brain reconstruction on the left). **d)** Cross correlation between cortical and subthalamic potentials for the subject in **c)**. Red region indicates significant cross correlation. **e)** Cortico-subthalamic lag during stopping, calculated using two analytic methods, showing that prefrontal potentials precede those in the STN. Using cross correlation, the distribution of lags for all cortico-subthalamic channel pairs had a median lag of  $-71 \pm 297$  ms (blue). In channels with clear ERP deflection onset, we calculated the offset between ERP deflections, and the median lag was  $-61 \pm 113$  ms (red). Boxplot on the right shows the distribution of mean cross correlation lags for each subject. **f)** Maximum correlation during stopping. All cortico-subthalamic channel pairs with significant cross correlation plotted in the left histogram, and boxplot on the right shows distribution of mean cross correlation values for each subject. **g)** The average cortico-subthalamic cross correlation during stopping is inversely correlated with estimated stop signal reaction time.

Within subjects, we looked for physiological predictors of behavior that would differentiate between successful and failed stop trials. We hypothesized three different models that could produce success versus failure: 1) IFG-STN activity is more correlated during successful stopping, 2) IFG-STN lag is shorter during successful stopping, or 3) IFG-STN activity is initiated more quickly during successful stopping. Within subjects, we did not find differences in cortico-subthalamic correlation ( $p=0.73$ , t-test; **Fig 2.8a**) or IFG-STN lag ( $p=0.93$ , t-test; **Fig 2.8b**) during successful versus failed stopping. We found that cortical ERPs during successful stopping preceded activity during failed stopping within subjects, with a mean lag of  $-12 \pm 21$  ms ( $p=0.050$ , one sample t-test; **Fig 2.8c**), suggesting that faster initiation of IFG-STN activity is important for successful stopping.

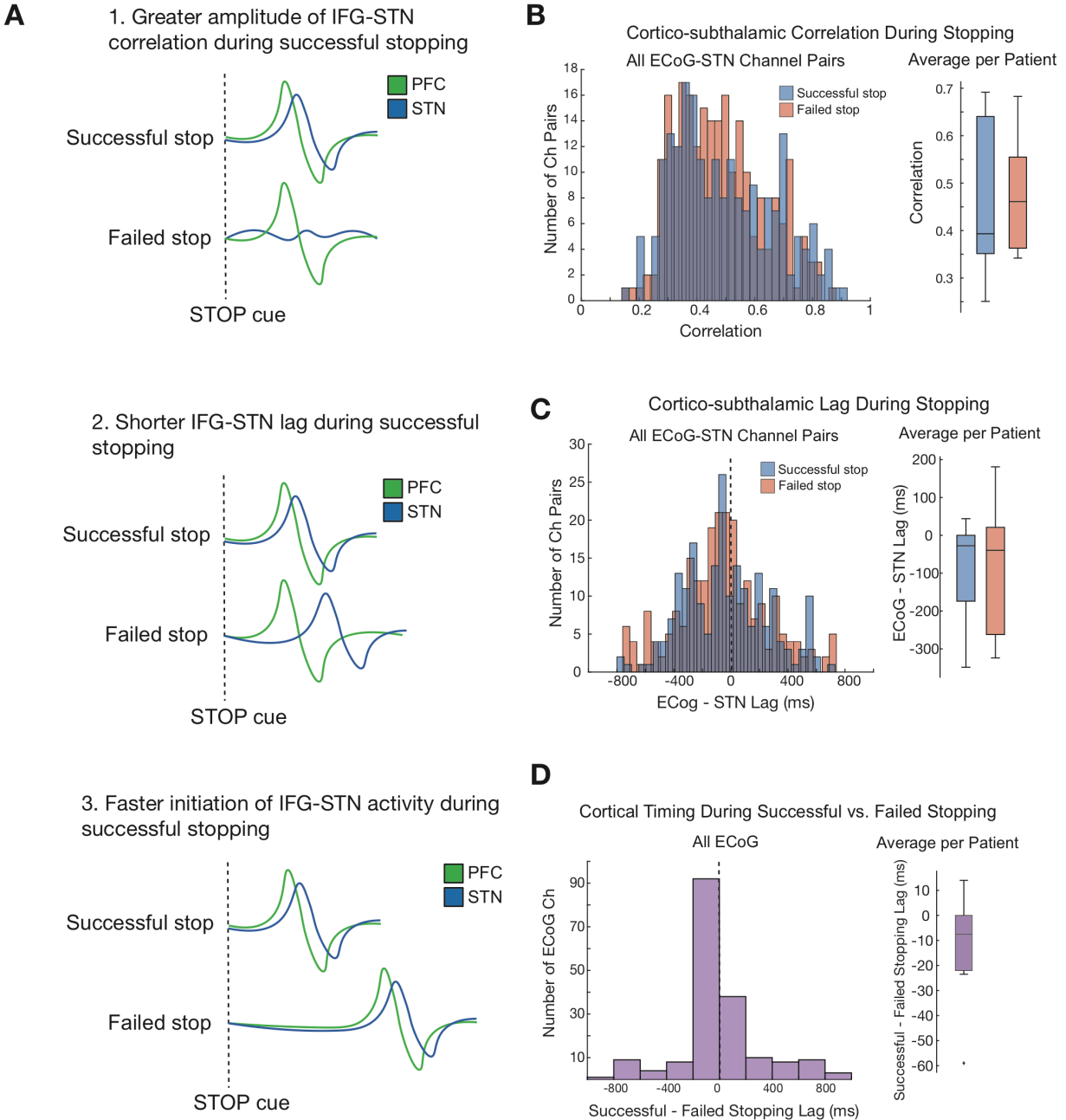


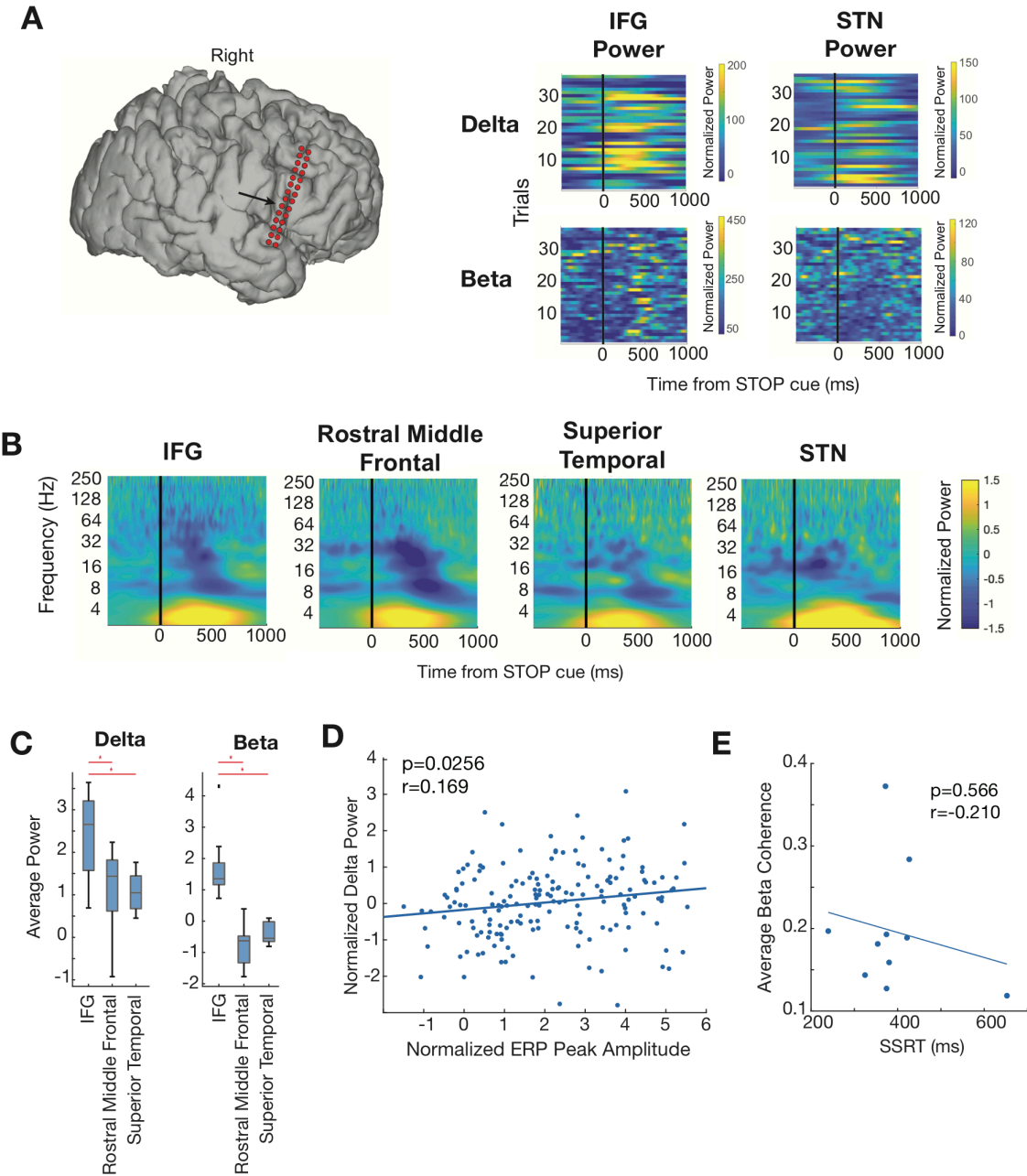
**Figure 2.8.** Within subjects, IFG-STN activity is initiated more quickly in successful versus failed stopping. **a)** Three schematics illustrating potential models of IFG-STN activity during successful versus failed stopping. **b)** Histograms of ECoG-STN correlation during successful versus failed stopping in all channel pairs (left) and average correlation per patient (right). There is no difference in successful versus failed stopping. **c)** Histograms of ECoG-STN lag during successful versus failed stopping in all channel pairs (left) and average lag per patient (right). There is no difference in successful versus failed stopping. **d)** Histograms of ECoG lag during successful versus failed stopping in all ECoG (left) and average lag per patient (right). Average lag is significantly different from zero.

### *IFG and STN modulate delta and beta frequencies during successful stopping*

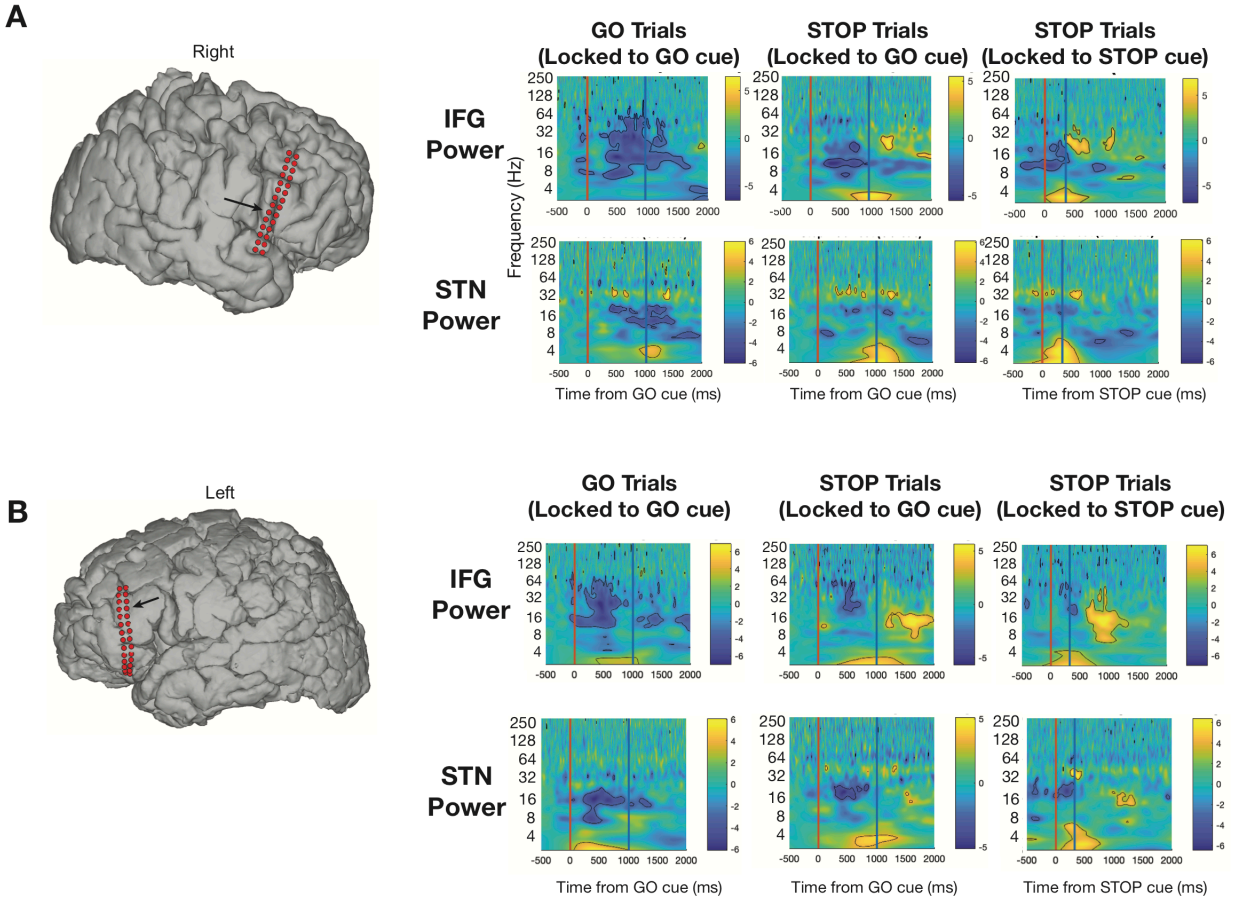
Previous studies characterizing single-site activity in either the IFG or the STN during stopping have linked modulations of beta power to successful stopping (Alegre et al., 2013; Kuhn et al., 2004; Ray et al., 2012; N. Swann et al., 2009; N. C. Swann et al., 2012). We therefore conducted frequency domain analyses to characterize stopping related oscillatory activity in the IFG and STN and stopping related coherence between these structures.

**Fig 2.9a** illustrates activity in a single cortical and single STN channel for an example patient. In single trials, delta activity in the IFG and STN increases immediately after the stop cue. The onset of delta power modulation has a consistent temporal relationship with the onset of the STOP cue, and it does not appear after the GO cue (**Fig 2.10a**), suggesting that it is a modulation specific to the stopping process. Beta power decreases after the GO cue, and then increases after the STOP cue in the IFG and STN (**Fig 2.9a, Fig 2.10a**). These delta and beta modulations were significant in the trial-averaged spectrograms (**Fig 2.10**). The increase in beta power occurred after the estimated time of stopping. Pooled activity across all subjects show similar modulations in the grand-averaged spectrograms (**Fig 2.9**). We used the grand average spectrograms to characterize the cortical topography of stopping-related activity. In the regions covered, the IFG had the greatest task-related delta and beta power ( $p < 0.05$  multifactorial ANOVA, with post-hoc Tukey's HSD pairwise comparisons; **Fig 2.9c**).

Since stopping-related delta activity in the frequency domain analyses is of short duration, it does not necessarily reflect an oscillatory phenomenon. This frequency domain modulation likely reflects the same ERP captured in the time domain. In support of this, task-evoked delta power was correlated with amplitude of the ERP ( $p = 0.03$ ,  $r = 0.17$ , Spearman correlation; **Fig 2.9d**).



**Figure 2.9.** Beta power is modulated during stopping, but IFG-STN beta coherence is not correlated with stopping behavior. **a**) In a single subject example, trial-by-trial modulation of delta (top) and beta (bottom) power during stopping, in the IFG (location indicated with arrow in brain reconstruction on the left) and STN. Trials are aligned to the STOP cue. **b**) Grand-averaged task-related spectrograms for all subjects. **c**) Quantification of task-related power modulation in the delta and beta frequencies for all subjects. Power in each frequency range was quantified in the 500 ms window surrounding each subject's stop signal reaction time. **d**) Correlation between stopping-related delta power and ERP peak amplitude for single ECoG channels. Delta power and ERP peak amplitudes are z-score normalized per patient. **e**) Average stopping-related beta coherence (in 500 ms window surrounding stop signal reaction time) is not correlated with stop signal reaction time.

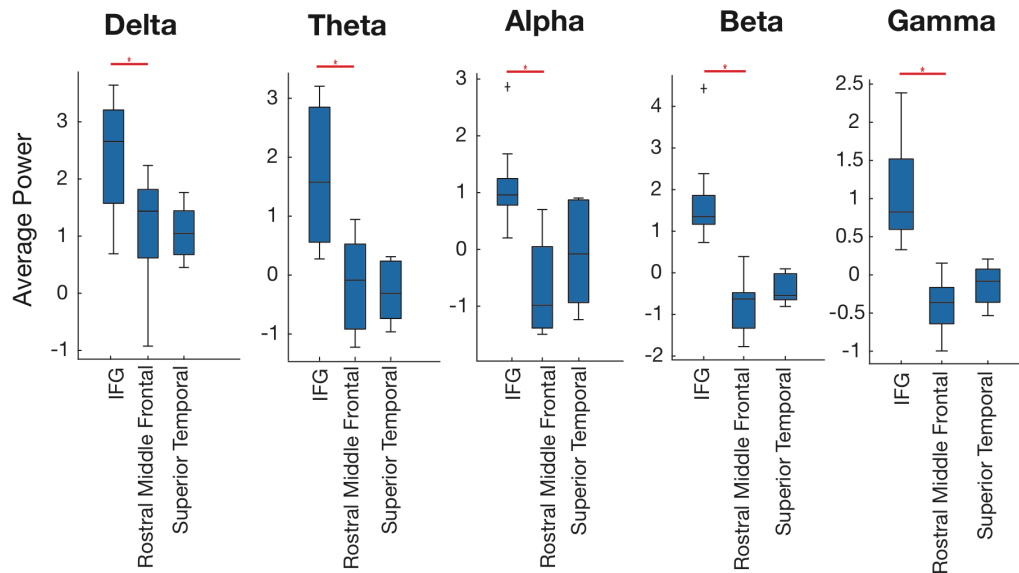
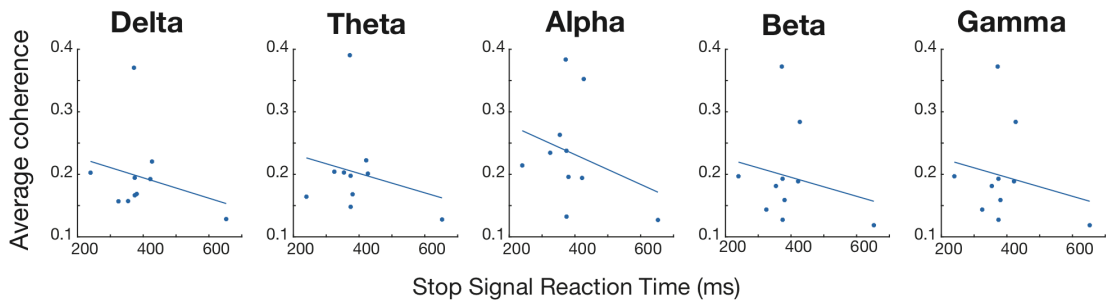


**Figure 2.10.** Qualitatively similar stopping-related activity in the right and left IFG. **a)** 3D reconstruction of ECoG location for a single patient with right ECoG. **b)** Trial-averaged activity in the IFG (top) and STN (bottom). Columns indicate trial type and cue for time-locking. Color indicates normalized power. Contoured regions indicate significant modulation (bootstrapping, false discovery rate corrected  $p < 0.05$ ).

Finally, we asked whether beta modulations in IFG and STN, or coherent beta band interactions between IFG and STN, predicted stopping behaviors, either between or within subjects. Beta power at each site individually, quantified in the 13-30 Hz range and in 250 ms window before and after the SSRT, was not predictive of SSRT (Bonferroni-corrected  $p > 0.05$ , Spearman correlation). Next, we analyzed beta in subject-specific narrow frequency bands, assessing beta amplitude and beta bursts in both the IFG and STN. Beta amplitude, burst rate, burst size, and burst duration (Hannah, Muralidharan, Sundby, & Aron, 2019) in both sites were not predictive of SSRT independently (Bonferroni-corrected  $p > 0.05$ , Spearman correlation), or in a combined multivariate regression model ( $p = 0.22$ ,  $R^2 = 0.35$ ). Within subjects, these metrics also did not differentiate successful versus failed stopping (Bonferroni-corrected  $p > 0.05$ , Wilcoxon signed rank). Furthermore, we did not find that beta amplitude or beta bursts were predictive of GO reaction times in either the IFG or STN (Bonferroni-corrected  $p > 0.05$ , Spearman correlation).

Oscillatory coherence between the IFG and STN was also not predictive of SSRT in the beta band ( $p = 0.57$ ,  $r = -0.21$ , Spearman correlation; **Fig 2.9e**), or in any other frequency range (**Fig 2.11**). We also looked for oscillatory interactions between IFG and STN by analyzing the power spectrum of the time-domain measure of synchronization discussed above, the cross correlation of the IFG and STN ERPs. These power spectra were calculated across all contact pairs then averaged for each patient. We found some patients with a visible peak in the beta band, consistent with an oscillatory coherence between prefrontal cortex and STN during stopping, though not all patients showed this peak (examples in **Fig 2.12**). However, there was no difference in SSRT between patients with and without a beta peak ( $p = 0.062$ , Wilcoxon rank sum). Thus, in this population of PD patients off of dopaminergic medication, we did not find evidence for a relationship between beta modulation and stopping or going in this circuit.



**A****B**

**Figure 2.11.** IFG-STN coherence during stopping is not related to stopping behavior. **a)** Quantification of power modulation in all subjects and in all frequency ranges during successful stopping. Multifactorial ANOVA with post-hoc Tukey's HSD,  $*p < 0.05$ . **b)** Correlation between stop signal reaction time and stopping-related coherence in all frequency ranges.

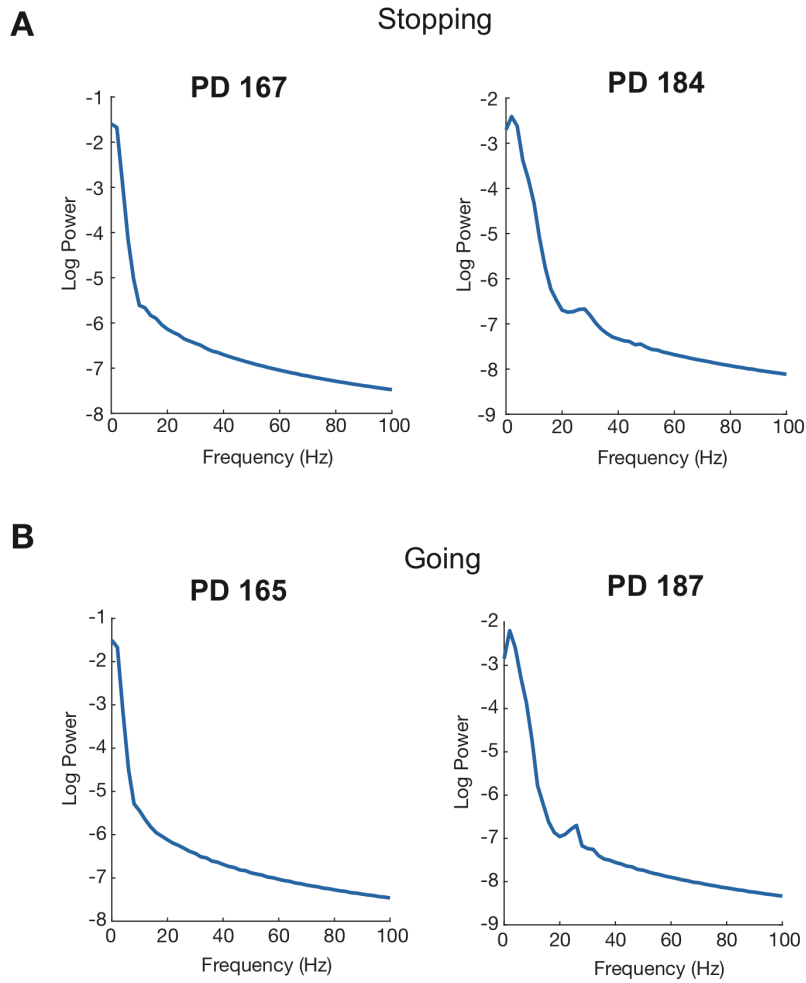


**Figure 2.12.** Power spectra of cortico-subthalamic cross correlograms, in 1 second window around stop and go signals, reveal beta peaks (local maxima) in some subjects but not all. **a)** Power spectra of cross correlograms during stopping for two example subjects. **b)** Power spectra of cross correlograms during going for two example subjects. To generate each plot, power spectra for cross correlations in all cortico-subthalamic contact pairs were calculated and averaged per patient. Power spectra on the left do not have a peak in the beta range, while those on the right do have a beta peak (by visual inspection).

## Discussion

We used invasive brain recordings in Parkinson's disease patients to characterize the IFG-STN circuit and its activity during stopping. By stimulating in the STN and recording in the prefrontal cortex, we identified a fast evoked potential that provides the first physiological evidence of hyperdirect (monosynaptic) connectivity between the IFG and ventral STN in humans. During a stop signal task, we show correlated stopping-related evoked activity in both the IFG and STN, and the degree of co-activation of these structures is predictive of stopping speed across subjects. Although we did find increases in IFG and STN beta at the estimated time of stopping, beta coherence was not correlated with stopping speed. Our study is the first to show that the hyperdirect circuit co-modulation is linked to stopping behaviors, which has broad implications for stimulation-based therapies to treat maladaptive movement inhibition.

### *Short latency evoked potentials identify a prefrontal-subthalamic hyperdirect pathway in humans*

The hyperdirect pathway was initially proposed to be a rapid connection from motor cortical regions to the STN, bypassing the striatum and providing rapid modulation of basal ganglia output (Atsushi Nambu et al., 2002). Subthalamic innervation from primary motor, supplementary motor, and premotor afferents was first identified in non-human primates using electrophysiological and histological techniques (Monakow, Akert, & Kunzle, 1978; A. Nambu, Takada, Inase, & Tokuno, 1996; Atsushi Nambu, Tokuno, Inase, & Takada, 1997). In humans, subthalamic stimulation elicits fast latency evoked potentials in *motor* cortical regions, recorded using EEG (Ashby et al., 2001; Baker et al., 2002; Walker et al., 2012) and ECoG (Kelley et al., 2018; Miocinovic et al., 2018), consistent with retrograde activation of a hyperdirect pathway. More recently, attention has focused on a possible *prefrontal*-subthalamic pathway and its role in the cognitive control of inhibition. Histological tracing in non-human primates have identified prefrontal projections to the STN, with a topography favoring more ventral regions of the STN

(Haynes & Haber, 2013). However, there has been limited anatomic or physiological characterization of this pathway in humans.

Our study is the first to use invasive electrodes at both the origin and the termination of the prefrontal-subthalamic hyperdirect pathway to show monosynaptic connectivity. Consistent with evoked potentials latencies reported in the EEG literature, we found an average latency of 2.2 ms for the earliest evoked event across all subjects. This evoked potential likely reflects rapid axonal back-propagation, with a conduction time of about 25 m/s, assuming a 5 cm distance between the prefrontal cortex and STN. These fibers are slower than the large axon fibers of corticospinal tract, which have conduction velocities of 41 m/s (Ashby, Strafella, Dostrovsky, Lozano, & Lang, 1998). This is consistent with rodent tract tracing studies showing that corticospinal fibers that collateralize to the STN have smaller diameter fibers than corticospinal axons that do not collateralize (T. Kita & Kita, 2012). We also found a longer latency evoked potential at 6 ms, suggesting hyperdirect fibers of different conduction velocities. Although a monosynaptic projection of opposite directionality (STN to cortex) has been identified histologically in rats (Degos, Deniau, Le Cam, Maily, & Maurice, 2008; Jackson & Crossman, 1981; H. Kita & Kitai, 1987), evoked potentials at 2 ms and 6 ms are too fast to include both axonal conduction and trans-synaptic events.

Using evoked potential amplitude as a surrogate metric for the density of axons extending from the cortex to the STN (Buzsaki, Anastassiou, & Koch, 2012), we found that IFG regions had preferential innervation with the faster hyperdirect fibers (2 ms latency) compared to neighboring regions, including the rostral middle frontal area and portions of the superior temporal lobe (**Fig 2.3c**). Evoked potentials from contacts covering superior temporal lobe likely arise from IFG activation within the Sylvian fissure rather than from the temporal lobe itself. The 6 ms evoked potential had a broader topographic distribution across the prefrontal cortex, consistent with nonhuman primate tracing studies suggesting broad prefrontal cortical innervation (Haynes & Haber, 2013). Furthermore, we found a topography of stronger prefrontal

projections to the ventral STN, consistent with anatomical (Haynes & Haber, 2013) and functional (Pasquereau & Turner, 2017) evidence from nonhuman primates. Dorsal STN stimulation did evoke the hyperdirect potential, but at a smaller amplitude. This may arise from current spread in this small nucleus, or from incomplete segregation of motor and nonmotor pathways (Haynes & Haber, 2013).

#### *IFG-STN hyperdirect pathway mediates rapid movement inhibition*

The IFG and STN are thought to be involved in stopping, but we have lacked precise physiological characterization of circuit activity during stopping in humans. Initial functional imaging studies found increased blood oxygenation in IFG, STN, and pre-SMA during successful stopping (Aron et al., 2007; Aron & Poldrack, 2006; C. D. Chambers, Garavan, & Bellgrove, 2009). Subsequent invasive studies in humans benefitted from higher temporal resolution recordings, but only had coverage of either the IFG or STN. In each site, assessed independently, successful stopping was associated with increased beta activity (Alegre et al., 2013; Kuhn et al., 2004; Ray et al., 2012; N. Swann et al., 2009; N. C. Swann et al., 2012), leading to the hypothesis that coherent beta activity between the IFG and STN mediates hyperdirect stopping.

We provide the first human evidence of IFG-STN communication consistent with hyperdirect modulation of stopping. First, the topography of stopping-related cortical activation coincided with that of hyperdirect connectivity, with both centered in the IFG (**Fig 2.9c**). Second, a task-evoked potential (probably corresponding to delta modulation in the frequency domain) appeared after the stop cue but before the estimated time of stopping. Cortical and subthalamic ERPs were highly correlated, with cortical activity leading the STN. Third, synchronization of evoked activity in the IFG and STN predicted faster stopping (**Fig 2.7g**), indicating a link between stopping behavior and activation of the hyperdirect pathway.

Similar to prior single site electrophysiology studies (Alegre et al., 2013; Kuhn et al., 2004; Ray et al., 2012; N. Swann et al., 2009; N. C. Swann et al., 2012), we also found increases in cortical and subthalamic beta band power during successful stopping. The beta modulation was strongest in IFG regions (**Fig 2.9c**). However, we did not find a relationship between IFG-STN coherence and stopping speed or successful versus failed stopping. In addition, stopping related beta increases in IFG tended to occur later than the estimated time of stopping, whereas an electrocorticography study in patients undergoing invasive monitoring for epilepsy showed an earlier onset of the stopping-related beta increase (N. Swann et al., 2009). While our data support a model in which IFG-STN interaction is mediated *primarily* by a fast evoked potential rather than by oscillatory synchronization, the parkinsonian state does perturb beta band activity in the classical thalamocortical motor loop (Brittain & Brown, 2014), and might likewise do so in the prefrontal cortex. This could reduce or delay a putative beta-band modulation of hyperdirect stopping. Although levodopa medication is not thought to affect SSRT (Obeso, Wilkinson, & Jahanshahi, 2011), our subjects' GO and STOP reaction times are slower than those previously reported, and Parkinson's disease is associated with deficits in behavioral inhibition (Frank, Samanta, Moustafa, & Sherman, 2007; Jahanshahi, Obeso, Baunez, Alegre, & Krack, 2015). Alternatively, if not causally involved in stopping, the beta modulation in the IFG and STN may reflect a rebound of activity related to action termination, which has been described in other regions involved in motor control, such as the sensorimotor cortex (Crone et al., 1998; Kuhn et al., 2004), supplementary motor area (Ohara, 2000), STN (Gauggel et al., 2004), and putamen (Sochurkova & Rektor, 2003).

The prefrontal hyperdirect pathway is likely to function as a brake during inhibitory processes beyond those probed in the stop signal task, such as during decision conflict (Frank et al., 2007; B. Zavala et al., 2016; B. A. Zavala et al., 2014) and during surprising events (Wessel & Aron, 2013). Thus a better understanding of the hyperdirect pathway is important for developing therapies to treat maladaptive behavioral inhibition, such as freezing of gait in

Parkinson's disease. Direct cortico-STN projections are thought to be perturbed in Parkinson's (Chu, McIver, Kovaleski, Atherton, & Bevan, 2017), and one therapeutic mechanisms of STN DBS is hypothesized to arise from altering hyperdirect activity (Gradinaru, Mogri, Thompson, Henderson, & Deisseroth, 2009). Modulation of stopping-related activity in this pathway may be therapeutic.

## CHAPTER 3

### PREFRONTAL ACTIVITY DURING EMOTIONAL FACE PROCESSING

#### **Abstract**

Parkinson's disease patients often experience non-motor symptoms including cognitive deficits, depression, and anxiety. Cognitive and affective processes are thought to be mediated by prefrontal cortico-basal ganglia circuitry. However, the topography and neurophysiology of prefrontal cortical activity during complex tasks are not well characterized. We used high-resolution electrocorticography in the prefrontal cortex of Parkinson's disease and essential tremor patients, during implantation of deep brain stimulator leads in the awake state, to understand disease-specific changes in prefrontal activity during an emotional face processing task. We found that Parkinson's patients had less task-related theta-alpha power and greater task-related gamma power in the dorsolateral prefrontal cortex, inferior frontal cortex, and lateral orbitofrontal cortex. These findings support a model of prefrontal neurophysiological changes in the dopamine-depleted state, in which focal areas of hyperactivity in prefrontal cortical regions may compensate for impaired long-range interactions mediated by low frequency rhythms. These distinct neurophysiological changes suggest that non-motor circuits undergo characteristic changes in Parkinson's disease.



## Introduction

Parkinson's disease is a movement disorder that is also characterized by non-motor symptoms, such as cognitive deficits, depression, and anxiety (K. R. Chaudhuri et al., 2006). These non-motor symptoms are an integral component of the disease itself, comprising the prodromal stage and advancing with disease progression (Schapira, Chaudhuri, & Jenner, 2017). A specific deficit in affective and cognitive functioning is the impaired ability to recognize emotional face images (Enrici et al., 2015; Wagenbreth, Wattenberg, Heinze, & Zaehle, 2016; Wieser et al., 2006). However, neural activity during emotional face recognition tasks in the dopamine-depleted state remains poorly understood.

Unlike non-motor circuits, the physiology of motor networks in Parkinson's have been studied extensively. High spatio-temporal resolution human brain recording techniques have informed the "oscillatory model" of the parkinsonian hypokinetic phenotype (de Hemptinne et al., 2013; de Hemptinne et al., 2015; Hammond et al., 2007). This model posits that cardinal motor signs of Parkinson's are related to changes in oscillatory synchronization within and between structures in the motor network. Electrocorticography (ECoG) and subcortical local field potential (LFP) recordings have been implemented acutely during deep brain stimulation (DBS) surgeries to study canonical motor regions (Panov et al., 2017). These methods have the capability of assessing low frequency rhythms important for inter-region communication (Fries, 2005, 2015), as well as broadband high frequency activity that assays local cortical activation at very fast time scales (Manning et al., 2009; Mukamel et al., 2005). However, these tools have not yet been widely applied to the study of non-motor circuits in Parkinson's disease.

Here we utilized high-resolution ECoG over lateral prefrontal and orbitofrontal regions, in patients undergoing surgery for DBS lead implantation in the awake state, to understand disease-specific changes in prefrontal cortical activity during an emotional face processing task. The prefrontal cortex is thought to be involved in cognitive and affective processes, including the appraisal of emotional stimuli (Carr et al., 2003; Fusar-Poli et al., 2009; Hariri et al., 2000;

Montgomery & Haxby, 2008; Phillips et al., 2003; Rolls, 2004). In order to determine whether Parkinson's is characterized by distinct prefrontal physiology during a complex task, we compared Parkinson's patients to a cohort of essential tremor patients. While essential tremor is also associated with psychiatric and other non-motor symptoms (Chandran & Pal, 2012; Lombardi, Woolston, Roberts, & Gross, 2001), they are generally milder than in Parkinson's and are unlikely to be connected to dopamine depletion. We found that Parkinson's patients had less task-related theta-alpha and more gamma activity during an emotional face processing task, suggesting prefrontal neurophysiological changes characteristic of the dopamine-depleted state.

## **Methods**

### *Subjects*

Subjects with idiopathic Parkinson's disease or essential tremor were recruited from the University of California San Francisco or the San Francisco Veterans Affairs Medical Center. Diagnoses were confirmed by movement disorders neurologists, and motor evaluations were conducted prior to DBS surgery using the Unified Parkinson's Disease Rating Scale (UPDRS) for Parkinson's patients. All Parkinson's patients had neuropsychiatric evaluations conducted by a psychiatrist or clinical psychologist as a part of routine clinical care. Inclusion criteria for Parkinson's patients included: primary rigid-akinetic motor phenotype, UPDRS-III  $\geq$  30, and motor fluctuations on versus off dopaminergic medications. Inclusion for essential tremor patients included tremor that was inadequately responsive to medication. All patients consented to have a temporary, subdural ECoG strip placed intraoperatively, during their DBS surgeries, on the prefrontal cortex for research purposes. All patients provided informed consent prior to surgery, per protocol approved by the Institutional Review Board.

### *DBS and ECoG placement*

Parkinson's patients had DBS electrodes targeted to the STN or globus pallidus internus (GPi) and essential tremor patients had DBS electrodes placed in the thalamic ventralis intermedius. DBS electrodes were placed under standard surgical protocol (Starr, 2002). A temporary, high-resolution, subdural ECoG strip (Ad-tech, Racine, WI) was inserted through the same burr hole used for DBS implantation (Panov et al., 2017). The 28-contact ECoG strip consisted of 2 rows of 14 contacts, and each contact was 1.2 mm in diameter, spaced 4 mm center-to-center. The strip was targeted to one of three prefrontal regions: dorsolateral prefrontal cortex (dlPFC), orbitofrontal cortex (OFC), or inferior frontal cortex (IFG). For unilateral DBS patients, the ECoG strip was placed ipsilateral to the DBS electrode, and for

bilateral DBS patients, ECoG was placed over the hemisphere contralateral to the first side implanted with a DBS lead. Targeting and placement were guided by surgical planning software (Medtronic Framelink v5.1, Minneapolis, MN), which provided image guidance with intraoperative CT fused to the preoperative MRI.

### *Electrode localization*

Postoperative image analyses were performed to localize each ECoG contact. FreeSurfer was used to reconstruct cortical surface models from the preoperative T1 MRI, and then the individual cortical surfaces were fit to the Desikan-Killiany atlas brain to generate cortical anatomy labels (Dale et al., 1999; Desikan et al., 2006; Fischl et al., 2002). The *img\_pipe* toolbox was used to fuse the intraoperative CT and preoperative MRI, project ECoG contacts onto the cortical surface mesh, and obtain the anatomic locations of each ECoG contact (Hamilton et al., 2017). We implemented an electrode projection method using surface vectors (Kubanek & Schalk, 2015), which visually minimized the distortion of projected strip electrodes and improved estimates of electrode location. Code for imaging analyses can be found at [https://github.com/MichaelLebrand/img\\_pype](https://github.com/MichaelLebrand/img_pype).

### *Emotional face processing task*

Subjects performed Tap That Emotion (Posit Science, San Francisco, CA), an emotional go/no-go task developed for the iPad (Apple, Cupertino, CA) (**Fig 3.1**). Six patients performed the task before DBS lead insertion and 6 patients after DBS lead insertion. An iPad was positioned 2 feet in front of the subject, and patients were presented with 50-100 images of emotional face images. 40% of trials were happy faces, 40% were sad faces, and 20% were neutral faces. Trial order was randomized. Subjects were instructed to identify the emotion type for each image and to respond as follows: for happy and sad faces, press a button on the iPad, and for neutral faces, withhold movement. Images were presented for 500 ms, with a variable

inter-trial interval between 500 and 1500 ms. The maximum period for response was 1000-2000 ms before the trial timed out. Of note, this task was designed to be easily and quickly performed in the stressful environment of the operating room, not to maximally challenge the subject with difficult or subtle distinctions.

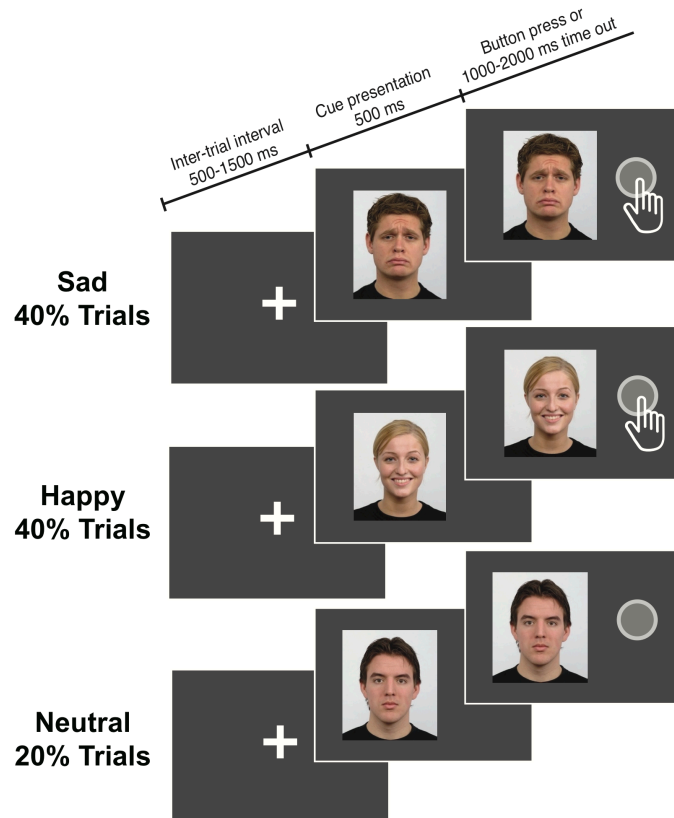


**Figure 3.1.** Emotional face processing task design. Subjects were instructed to identify the emotional valence of the image and to respond with a button press for sad and happy faces, but not for neutral faces.

### *Signal recordings*

ECoG potentials were recorded on the Neuro Omega (Alpha Omega, Nazareth, Israel) or the TDT PZ5 (Tucker Davis Technologies, Alachua, FL) acquisition systems. The Neuro Omega signals are recorded at a 22 KHz sampling rate and 0.075-3500 Hz bandpass filtered. The TDT signals are recorded at 3 kHz and 0.45-1350 Hz bandpass filtered. All ECoG potentials were recorded referenced to an ipsilateral scalp needle, which was placed subcutaneously over the vertex.

### *Neural data analysis*

Custom MATLAB scripts were used to analyze electrophysiology data. Task-related data were downsampled to 1000 Hz. Spectral power at rest was calculated using the Welch periodogram method using a Fast Fourier Transform of 512 points. Task-related spectrograms were generated using wavelets (Canolty et al., 2007). In a single patient, ECoG potentials for each channel were filtered with Gabor Wavelets into 128 center frequencies ranging from 2.5-250 Hz. Epochs of data were time-locked to the image onset of each trial, and all epochs were averaged. Each frequency in the spectrogram was baseline corrected by subtracting the average power of the 500 ms preceding the cue, corresponding to the inter-trial interval. Spectrograms were z-score normalized with bootstrapping. First, a distribution of 10,000 surrogate spectrograms were generated using permutations of the task spectrograms at random time points. Then, each point on the task spectrogram was transformed into a z-score using the mean and standard deviation generated from the surrogate spectrogram distribution. Within patients, an average spectrogram per anatomic region was calculated by averaging all contacts within the same region. All trial types (happy, sad, and neutral face images) were included. Grand averaged spectrograms were generated by averaging patients. To quantify task-related power, the average value of task-related power from image onset (0 ms) to the mean reaction

time for all patients was calculated for the following frequency ranges: delta (1-4 Hz), theta (4-8 Hz), alpha (8-13 Hz), beta (13-30 Hz), low gamma (30-50 Hz), and high gamma (50-150 Hz).

### *Statistical Analyses*

Factorial analyses of variance (ANOVA) were performed to compare task-related power between disease groups and between anatomic regions. Post-hoc Bonferonni tests were conducted for pair-wise comparisons. A Bonferonni corrected p-value <0.05 was considered statistically significant for grouped data.

## Results

### *Subjects*

Twelve patients were enrolled in this study: 7 Parkinson's (3 male/4 female) and 5 essential tremor (4 male/1 female) subjects (**Table 3.1**). The mean age of the Parkinson's and essential tremor patients were  $61.7 \pm 10.0$  years and  $69.0 \pm 6.4$  years, respectively. The average disease duration for Parkinson's patients was  $8.1 \pm 4.6$  years and for essential tremor patients was  $35.0 \pm 12.8$  years. Four out of 7 Parkinson's subjects and 2 out of 5 essential tremor subjects were prescribed medications for psychiatric symptoms (**Table 3.1**).

ECoG potentials were recorded from the right hemisphere in 7 patients and from the left hemisphere in 5 patients. A total of 300 ECoG electrodes covering the frontal lobe were analyzed (**Table 3.2; Fig 3.2a**). Forty one electrodes were on the IFG pars triangularis, 56 electrodes on the IFG pars orbitalis, 167 electrodes on the superior frontal gyrus (dIPFC), and 36 electrodes on the lateral OFC. In 4 subjects, a total of 36 channels were not included in the analyses due to electrical noise or equipment failure during recording.



**Table 3.1.** Patient characteristics in emotional face processing study

	Age	Sex	Disease Duration (years)	UPDRS-III ON/OFF Meds	ECoG Side	DBS Target	PAS	BDI	MOCA	Psychiatric Medications
<b>ET 039</b>	68	M	40	--	R	Vim	--	--	--	--
<b>ET 040</b>	70	M	54	--	L	Vim	--	--	25	Buspirone, Citalopram, Quetiapine
<b>ET 047</b>	60	F	31	--	R	Vim	--	--	--	Clonazepam
<b>ET 048</b>	69	M	40	--	R	Vim	--	--	--	--
<b>ET 049</b>	78	M	20	--	L	Vim	--	--	--	None
<b>PD 100</b>	72	M	6	16/28	R	STN	--	9	29	Clonazepam
<b>PD 119</b>	52	F	14	29/60	L	STN	7	--	26	None
<b>PD 121</b>	56	F	6	5/31	L	STN	10	12	24	Bupropion, Alprazolam
<b>PD 123</b>	47	M	5	21/39	R	GPI	19	18	23	Escitalopram
<b>PD 153</b>	71	F	8	9/33	R	STN	8	10	21	None
<b>PD 155</b>	69	F	15	7/16	R	STN	3	--	24	None
<b>PD 162*</b>	65	M	3	21/41	L	STN	17	14	25	Citalopram, Gabapentin, Trazodone

ET = essential tremor; PD = Parkinson's disease; UPDRS-III = Unified Parkinson's Disease Rating Scale Part III; PAS = Parkinson's Anxiety Scale; BDI = Beck Depression Inventory; MOCA = Montreal Cognitive Assessment

**Table 3.2.** Electrode locations in emotional face processing study

	Number of ECoG Contacts			
	IFG pars triangularis	IFG pars orbitalis	Dorsolateral prefrontal cortex	Lateral orbitofrontal cortex
ET 039	0	11	0	17
ET 040	9	13	1	5
ET 047	0	0	27	0
ET 048	1	2	22	0
ET 049	0	0	28	0
PD 100	0	5	23	0
PD 119	0	1	27	0
PD 121	0	0	11	1
PD 123	0	4	12	0
PD 153	11	10	1	6
PD 155	10	10	1	7
PD 162*	10	0	14	0

ET = essential tremor; PD = Parkinson's disease; IFG = inferior frontal cortex.

\*ECoG channels not located on the prefrontal cortex were excluded from these analyses

*Parkinson's disease patients have reduced prefrontal theta-alpha and increased prefrontal gamma activity during an emotional face processing task*

Behaviorally, Parkinson's and essential tremor patients performed similarly on the emotional face processing task. Mean reaction times for Parkinson's and essential tremor patients were  $968 \pm 287$  ms and  $1139 \pm 201$  ms, respectively, and mean task accuracy was  $72 \pm 14\%$  and  $72 \pm 16\%$  respectively. There were no statistical differences in reaction time (Wilcoxon rank sum,  $p=0.27$ ) or task accuracy (Wilcoxon rank sum,  $p=0.96$ ) between the two groups. We compared ECoG potentials between Parkinson's and essential tremor patients at rest and during the emotional face processing task (**Fig 3.2b,c**). At baseline during rest, there were no differences in prefrontal spectral power in any frequency range (Wilcoxon rank sum; **Fig 3.3a**). To compare task-related cortical physiology between the two groups, we computed the grand averaged spectrograms time-locked to cue presentation. We quantified task-related activity per frequency band from cue presentation to all patients' average reaction time, 1039 ms. PD patients have lower task-related low frequency activity in the theta band ( $F(1,21)=5.87$ ,  $p=0.0246$ ; **Fig 3.3b,c**) and alpha band ( $F(1,21)=4.75$ ,  $p=0.0409$ ; **Fig 3.3b,c**). PD patients also had greater task-related prefrontal high gamma than ET patients ( $F(1,21)=4.73$ ,  $p=0.0412$ ; **Fig 3.3b,c**). The main effect was driven by disease, and there were no significant interactions between disease and cortical location in any frequency range. We assessed whether the task-related high gamma had a topographic focality in the prefrontal cortex. We found that task-related high gamma was not restricted to individual contacts of the 28 contact strip and occurred over a broad cortical region (**Fig 3.4a,b**).

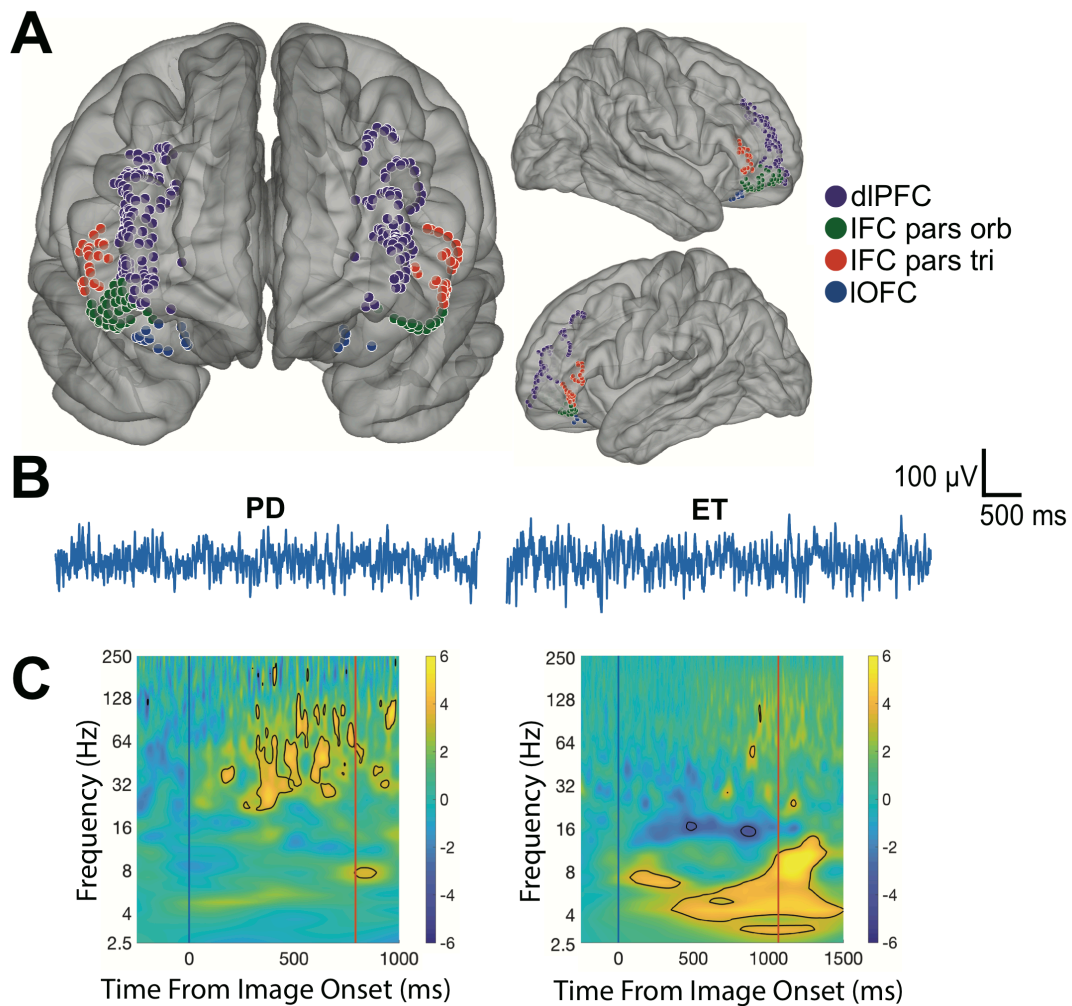


**Figure 3.2.** High-resolution ECoG in Parkinson's and essential tremor patients. **a)** 3D reconstruction of prefrontal ECoG contact locations for all patients, projected onto an atlas brain. **b)** Sample resting ECoG potentials in a single ECoG channel for a Parkinson's (left) and essential tremor (right) patient. **c)** Sample task-related spectrograms for a single ECoG channel in a PD (left) and ET (right) patient during emotional face processing task. Activity is time-locked to image onset at 0 ms, and the red line marks each patient's average reaction time. All trials are averaged. Color axis indicates z-score normalized power values. Outlined areas highlight regions of significant task-related activity corresponding to an FDR-corrected  $p < 0.01$ .

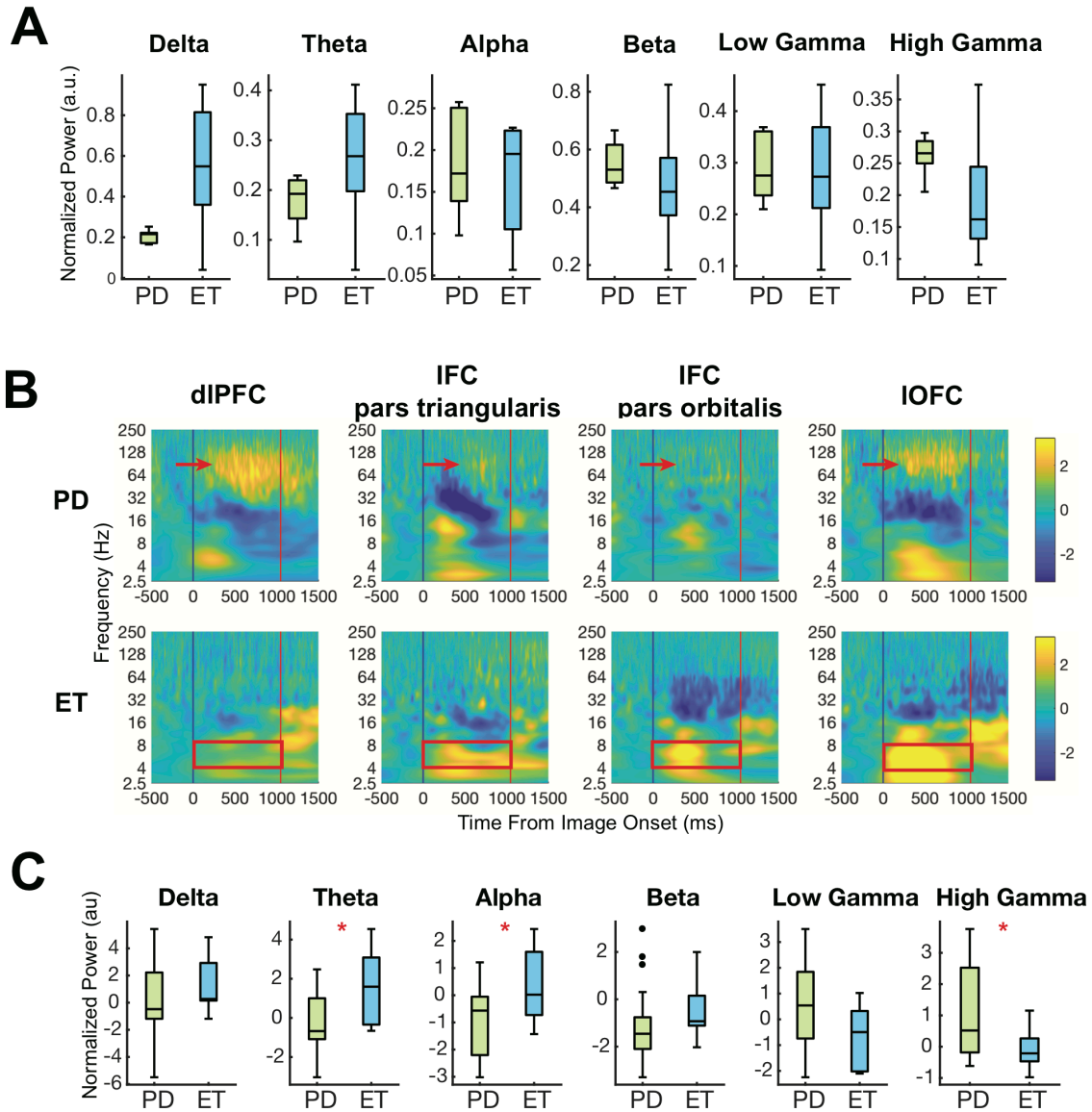


**Figure 3.3.** Disease-specific alterations in task-related theta/alpha and high gamma activity. **a)** Quantification of spectral power during baseline at rest. Spectral power for 1 minute of resting data was calculated per patient, and all ECoG contacts were averaged within a patient. Power per frequency range was normalized to total power between 5-55 Hz (delta, theta, alpha, beta) or 65-100 Hz (low gamma, high gamma). **b)** Grand averaged spectrograms of task-related activity during emotional face processing task in PD (top row) versus ET (bottom row) patients, per anatomic region. Spectrograms are aligned to image onset at 0 ms. Red line at 1039 ms indicates the average reaction time for all patients. **c)** Quantification of spectral power during the emotional face processing task. The average power per frequency range was calculated from 0-1039 ms. Parkinson's patients had lower task-related theta ( $p=0.0246$ ) and alpha ( $p=0.0409$ ), as well as greater high gamma ( $p=0.0412$ ).

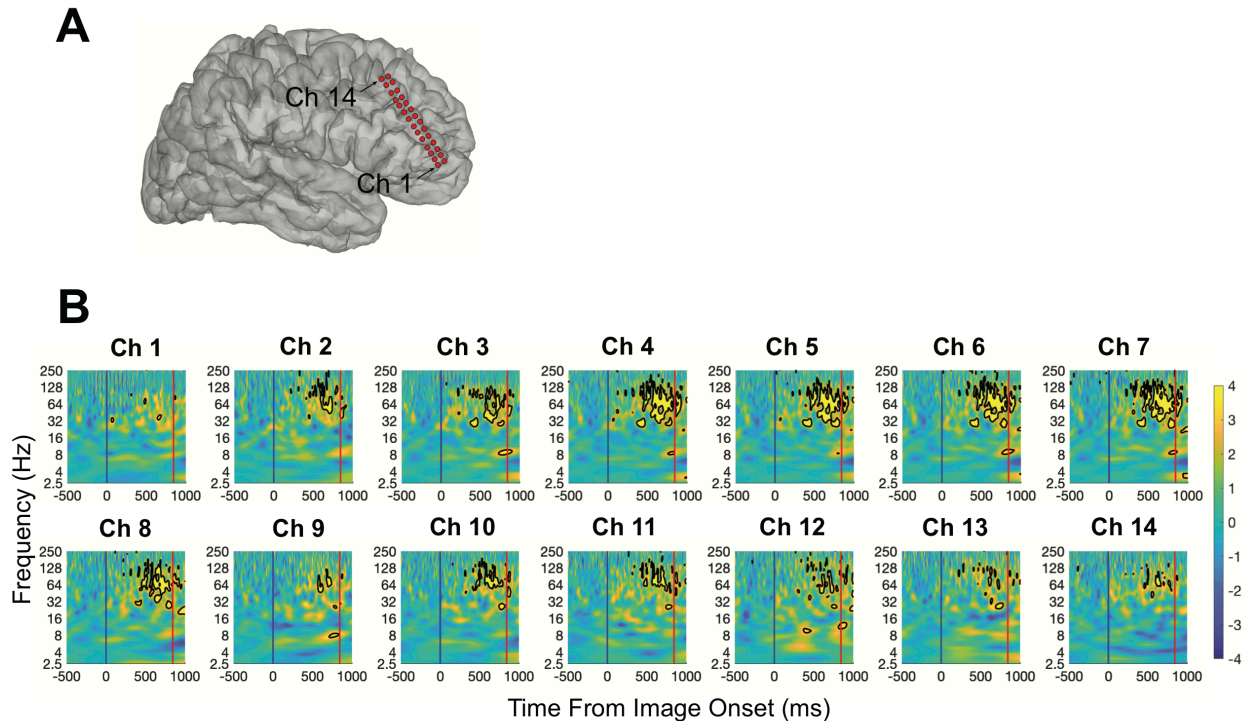


**Figure 3.4.** No topographic focality in task-related high gamma activity during emotional face processing. **a)** 3D reconstruction of ECoG strip location for a single Parkinson's patient. **b)** Task-related spectrograms for one row of ECoG channels, all trials averaged. Outlined areas highlight regions of significant task-related activity corresponding to a false discovery rate-corrected  $p < 0.01$ .

We then assessed whether there were differences in prefrontal cortical physiology in response to the different emotional valences of the stimuli. We generated spectrograms for happy, sad, and neutral images per subject, and then averaged subjects together for the valence-specific grand spectrograms. To control for the differences in trial numbers per trial type, we randomly subselected a constant number of trials to generate valence-specific spectrograms for each subject. We found no differences in prefrontal task-related activity by trial type (data not shown).

## Discussion

We utilized high-resolution intraoperative ECoG, in patients undergoing DBS implantation in the awake state, to characterize prefrontal activity during an emotional face processing task in Parkinson's and essential tremor patients. We targeted the dlPFC, IFG, and OFC because functional imaging studies have implicated these regions of the prefrontal cortex in emotional and cognitive processing (Carr et al., 2003; Fusar-Poli et al., 2009; Hariri et al., 2000; Montgomery & Haxby, 2008; Phillips et al., 2003; Rolls, 2004). In all regions studied, we found that Parkinson's patients have lower theta-alpha and greater high gamma during an emotional face processing task compared to essential tremor patients. Our results show that the dopamine-depleted state is associated with distinct prefrontal neurophysiology during an emotional face processing task, suggesting that cognitive and affective circuits may undergo disease-specific changes in Parkinson's disease.

### *Deficit in theta reactivity may affect circuit integration in non-motor networks*

The emotional face processing task likely recruits various simultaneous processes for attention recruitment, assessment of emotional valence, conflict resolution, decision-making, and motor output generation or inhibition. The neural circuits underlying these processes must be synchronized to complete the task properly. Low frequency oscillations are thought to synchronize neural networks by temporally coordinating excitability in different brain regions. This mechanism, known as "communication through coherence," permits integration of distributed brain areas required to perform complex tasks (Fries, 2005, 2015). Functional connectivity between the prefrontal cortex and other brain structures, such as the amygdala, is required for emotional processing and regulation (Gold, Morey, & McCarthy, 2015; S. Wang et al., 2017). The prefrontal cortex exerts top-down control of stimulus processing (Gold et al., 2015) and these top-down control mechanisms may be mediated by inter-region theta coherence (Herz et al., 2017; B. A. Zavala et al., 2014). In cognitive networks, theta oscillations

have been shown to orchestrate prefrontal cortical and subcortical structures during learning, memory, and attentional processes (Benchenane, Tiesinga, & Battaglia, 2011; Cavanagh & Frank, 2014; Cavanagh et al., 2011). In Parkinson's, theta is similarly involved in complex cognitive functions including conflict and error monitoring, particularly between the medial prefrontal cortex and STN (Kelley et al., 2018; B. Zavala et al., 2016). Furthermore, scalp EEG recording in humans with Parkinson's disease (Singh, Richardson, Narayanan, & Cavanagh, 2018) and optogenetic studies in rodent models (Kim et al., 2017; Parker, Chen, Kingyon, Cavanagh, & Narayanan, 2015) show that mid-frontal theta in the dopamine-depleted state is diminished during cognitive control, suggesting that deficits in low frequency modulation may underlie cognitive deficits in Parkinson's disease.

Consistent with a prominent role for theta band activity in non-motor functioning, we show prefrontal theta modulation during an emotional face processing task that invokes a variety of cognitive and affective processes. The task-related increase in theta-alpha frequencies was diminished in Parkinson's patients compared to essential tremor patients, and this attenuated prefrontal theta reactivity in Parkinson's may reflect a disease-specific deficit arising from dopamine depletion. Given the diverse roles of the prefrontal cortex, the deficits in theta reactivity in Parkinson's may produce impairments in the recognition and regulation of emotional states, as well as in cognitive processes required to perform task. The involvement of theta oscillations in parkinsonian non-motor functioning suggests new therapeutic strategies aimed at restoring task-related theta increases. In non-parkinsonian patients with depression, for example, deep brain stimulation in the limbic striatum boosts theta activity during a cognitive task performed in the presence of emotional distractors and improves task performance (Widge et al., 2019).



*Parkinson's disease patients may compensate for oscillatory deficits by excessive activation of the prefrontal cortex*

In healthy subjects, functional imaging studies suggest that various prefrontal regions are engaged during emotional processing tasks, but there is no consensus on topography (Phan, Wager, Taylor, & Liberzon, 2002). Behaviorally, Parkinson's patients have deficits in the ability to assess the valence of emotional face images (Enrici et al., 2015; Wagenbreth et al., 2016; Wieser et al., 2006). Assessments of gray matter volume in Parkinson's patients suggest that bilateral OFC gray matter volume is positively correlated with facial emotion recognition performance (Ibarretxe-Bilbao et al., 2009). Furthermore, functional imaging suggests compensatory prefrontal activity to counteract behavioral deficits. Subclinical *Parkin* mutation carriers have a hyperactive right pars opercularis during emotional face processing (Anders et al., 2012) and symptomatic Parkinson's patients have a hyperactive medial prefrontal cortex while processing arousing emotional images (Moonen et al., 2017). Although functional imaging studies have comprehensive spatial coverage of the brain, they lack temporal resolution.

Utilizing electrophysiological tools that can assess neural activity at fast time scales, our findings support imaging evidence of Parkinson's prefrontal hyperactivity during an emotional face processing task. We used cortical high gamma power as a surrogate metric for local neuronal activity, as it has been shown to correlate with fMRI BOLD and also with population spiking (Logothetis, Pauls, Augath, Trinath, & Oeltermann, 2001; Manning et al., 2009; Mukamel et al., 2005). We found greater task-related gamma in Parkinson's patients compared to essential tremor patients in the IFG pars triangularis, IFG pars orbitalis, dlPFC, and lateral OFC, suggesting a hyperactive prefrontal cortex. The area of prefrontal cortex over which this disease-specific gamma band activation occurred serves diverse cognitive functions (Duncan & Owen, 2000). These power spectral changes may reflect a change in the balance between cortical excitation and inhibition (Gao, Peterson, & Voytek, 2017).

Prefrontal theta-gamma coupling in rodent models have been shown to be modulated by dopaminergic input to the prefrontal cortex (Lohani, Martig, Deisseroth, Witten, & Moghaddam, 2019). In the dopamine-depleted state, we propose that prefrontal hyperactivity stems from compensatory mechanisms to overcome the deficit in low frequency network oscillations involved in cognitive and affective processing. Given the demonstrated role of prefrontal control in movement inhibition (Aron et al., 2016), an alternative hypothesis is that the Parkinson's-specific pattern of gamma activation in our study is related to the movement inhibition/activation element of the task, rather than emotional face processing. However, we do not see similar task-evoked gamma activity in two subjects who performed a non-emotional go/no-go task with a similar cortical recording paradigm (data not shown).

### *Limitations*

Due to the invasive nature of our study, Parkinson's disease patients were compared to essential tremor patients instead of healthy controls. Although non-motor symptoms may occur in both disease groups, comorbid psychiatric states are more common in Parkinson's, and dopamine depletion is specific to Parkinson's. In our cohort, comprehensive neuropsychiatric evaluations are not a part of routine clinical care for essential tremor patients. Limited intraoperative research time restricted our tasks to simple designs and low trial numbers, which did not allow us to establish differences in task performance potentially due to ceiling effects. Our findings suggest that prefrontal physiology in Parkinson's and essential tremor patients are distinct despite employing a task that was simple enough to evoke similar task performance. In some patients, recordings were performed after DBS lead insertion, which may produce "microlesional" effects. However, similar task-related activity was seen in pre-lead and post-lead patients (data not shown). The relatively low number of trials that can be done in the intraoperative environment precluded subgroup analyses of cortical responses to stimuli of different emotional valences. Therefore, we cannot attribute task-related activity specifically to

emotional face processing, as the neurophysiological modulations may reflect a variety of cognitive and affective processes. We grouped Parkinson's and essential tremor patients who had ECoG recorded in both left and right hemispheres, as we did not have sufficient patients to statistically analyze laterality within disease groups. However, we found similar activity in both the left and right prefrontal cortex (data not shown).

### *Summary*

The effect of the parkinsonian state on the neurophysiology of the prefrontal cortex during complex cognitive and affective tasks has been underexplored. Utilizing intracranial recordings during an emotional face processing task in Parkinson's and essential tremor patients, we demonstrate Parkinson's disease-specific changes in low frequency oscillatory activity as well as high gamma broadband activity. This work suggests that the "oscillation model" of the motor system in Parkinson's, widely used to explain specific motor deficits, may also extend to prefrontal cortical areas that contribute to non-motor deficits.

## CHAPTER 4

### CONCLUSIONS

The results presented in this dissertation expand our understanding of prefrontal cortical functioning in Parkinson's disease. Specifically, we characterized prefrontal activity during movement inhibition and during emotional stimuli processing in humans.

In Chapter 2, we assessed the topography and function of the prefrontal-subthalamic hyperdirect pathway. We found monosynaptic connectivity between broad prefrontal cortical regions and the subthalamic nucleus, with the fastest fibers originating in the inferior frontal regions. We showed co-activation of the inferior frontal gyrus and subthalamic nucleus during stopping, and the degree of this co-activation was correlated with the stopping speed. These results establish the first human evidence of hyperdirect connectivity between the prefrontal cortex and subthalamic nucleus, and we show how this circuit is modulated during movement inhibition.

In Chapter 3, we characterized prefrontal activity during emotional face processing. We compared Parkinson's patients with essential tremor patients to find disease-specific changes in prefrontal activity during affective processing. We found prefrontal hyperactivity during the appraisal of emotional face images, which was specific to the dopamine-depleted state. These results suggest that cognitive and affective circuits may undergo disease-specific changes in Parkinson's disease.

## REFERENCES

- Alegre, M., Lopez-Azcarate, J., Obeso, I., Wilkinson, L., Rodriguez-Oroz, M. C., Valencia, M., . . . Obeso, J. A. (2013). The subthalamic nucleus is involved in successful inhibition in the stop-signal task: a local field potential study in Parkinson's disease. *Exp Neurol*, *239*, 1-12. doi:10.1016/j.expneurol.2012.08.027
- Anders, S., Sack, B., Pohl, A., Munte, T., Pramstaller, P., Klein, C., & Binkofski, F. (2012). Compensatory premotor activity during affective face processing in subclinical carriers of a single mutant Parkin allele. *Brain*, *135*(Pt 4), 1128-1140. doi:10.1093/brain/aws040
- Aron, A. R., Behrens, T. E., Smith, S., Frank, M. J., & Poldrack, R. A. (2007). Triangulating a cognitive control network using diffusion-weighted magnetic resonance imaging (MRI) and functional MRI. *J Neurosci*, *27*(14), 3743-3752. doi:10.1523/JNEUROSCI.0519-07.2007
- Aron, A. R., Herz, D. M., Brown, P., Forstmann, B. U., & Zaghoul, K. (2016). Frontosubthalamic Circuits for Control of Action and Cognition. *J Neurosci*, *36*(45), 11489-11495. doi:10.1523/JNEUROSCI.2348-16.2016
- Aron, A. R., & Poldrack, R. A. (2006). Cortical and subcortical contributions to Stop signal response inhibition: role of the subthalamic nucleus. *J Neurosci*, *26*(9), 2424-2433. doi:10.1523/JNEUROSCI.4682-05.2006
- Ashby, P., Paradiso, G., Saint-Cyr, J. A., Chen, R., Lang, A. E., & Lozano, A. M. (2001). Potentials recorded at the scalp by stimulation near the human subthalamic nucleus. *Clinical Neurophysiology*, *112*(3), 431-437. doi:10.1016/s1388-2457(00)00532-0
- Ashby, P., Strafella, A., Dostrovsky, J. O., Lozano, A., & Lang, A. E. (1998). Immediate motor effects of stimulation through electrodes implanted in the human globus pallidus. *Stereotact Funct Neurosurg*, *70*(1), 1-18. doi:10.1159/000029593

- Baker, K. B., Montgomery, E. B., Jr., Rezai, A. R., Burgess, R., & Luders, H. O. (2002). Subthalamic nucleus deep brain stimulus evoked potentials: physiological and therapeutic implications. *Mov Disord*, *17*(5), 969-983. doi:10.1002/mds.10206
- Benchenane, K., Tiesinga, P. H., & Battaglia, F. P. (2011). Oscillations in the prefrontal cortex: a gateway to memory and attention. *Curr Opin Neurobiol*, *21*(3), 475-485. doi:10.1016/j.conb.2011.01.004
- Brittain, J. S., & Brown, P. (2014). Oscillations and the basal ganglia: motor control and beyond. *Neuroimage*, *85 Pt 2*, 637-647. doi:10.1016/j.neuroimage.2013.05.084
- Buzsaki, G., Anastassiou, C. A., & Koch, C. (2012). The origin of extracellular fields and currents--EEG, ECoG, LFP and spikes. *Nat Rev Neurosci*, *13*(6), 407-420. doi:10.1038/nrn3241
- Buzsaki, G., & Draguhn, A. (2004). Neuronal oscillations in cortical networks. *Science*, *304*(5679), 1926-1929. doi:10.1126/science.1099745
- Canolty, R. T., Ganguly, K., Kennerley, S. W., Cadieu, C. F., Koepsell, K., Wallis, J. D., & Carmena, J. M. (2010). Oscillatory phase coupling coordinates anatomically dispersed functional cell assemblies. *Proc Natl Acad Sci U S A*, *107*(40), 17356-17361. doi:10.1073/pnas.1008306107
- Canolty, R. T., & Knight, R. T. (2010). The functional role of cross-frequency coupling. *Trends Cogn Sci*, *14*(11), 506-515.
- Canolty, R. T., Soltani, M., Dalal, S. S., Edwards, E., Dronkers, N. F., Nagarajan, S. S., . . . Knight, R. T. (2007). Spatiotemporal dynamics of word processing in the human brain. *Front Neurosci*, *1*(1), 185-196. doi:10.3389/neuro.01.1.1.014.2007
- Carr, L., Iacoboni, M., Dubeau, M. C., Mazziotta, J. C., & Lenzi, G. L. (2003). Neural mechanisms of empathy in humans: a relay from neural systems for imitation to limbic areas. *Proc Natl Acad Sci U S A*, *100*(9), 5497-5502. doi:10.1073/pnas.0935845100

- Cavanagh, J. F., & Frank, M. J. (2014). Frontal theta as a mechanism for cognitive control. *Trends Cogn Sci*, 18(8), 414-421. doi:10.1016/j.tics.2014.04.012
- Cavanagh, J. F., Wiecki, T. V., Cohen, M. X., Figueroa, C. M., Samanta, J., Sherman, S. J., & Frank, M. J. (2011). Subthalamic nucleus stimulation reverses mediofrontal influence over decision threshold. *Nat Neurosci*, 14(11), 1462-1467. doi:10.1038/nn.2925
- Chambers, C. D., Bellgrove, M. A., Stokes, M. G., Henderson, T. R., Garavan, H., Robertson, I. H., . . . Mattingley, J. B. (2006). Executive "Brake Failure" following Deactivation of Human Frontal Lobe. *Journal of Cognitive Neuroscience*, 18(3), 444-455. doi:10.1162/jocn.2006.18.3.444
- Chambers, C. D., Garavan, H., & Bellgrove, M. A. (2009). Insights into the neural basis of response inhibition from cognitive and clinical neuroscience. *Neurosci Biobehav Rev*, 33(5), 631-646. doi:10.1016/j.neubiorev.2008.08.016
- Chandran, V., & Pal, P. K. (2012). Essential tremor: beyond the motor features. *Parkinsonism Relat Disord*, 18(5), 407-413. doi:10.1016/j.parkreldis.2011.12.003
- Chaudhuri, K. R., Healy, D. G., Schapira, A. H., & National Institute for Clinical, E. (2006). Non-motor symptoms of Parkinson's disease: diagnosis and management. *Lancet Neurol*, 5(3), 235-245. doi:10.1016/S1474-4422(06)70373-8
- Chaudhuri, K. R., & Schapira, A. H. V. (2009). Non-motor symptoms of Parkinson's disease: dopaminergic pathophysiology and treatment. *The Lancet Neurology*, 8(5), 464-474. doi:10.1016/s1474-4422(09)70068-7
- Chu, H. Y., Mclver, E. L., Kovaleski, R. F., Atherton, J. F., & Bevan, M. D. (2017). Loss of Hyperdirect Pathway Cortico-Subthalamic Inputs Following Degeneration of Midbrain Dopamine Neurons. *Neuron*, 95(6), 1306-1318 e1305. doi:10.1016/j.neuron.2017.08.038
- Crone, N. E., Miglioretti, D. L., Gordon, B., Sieracki, J. M., Wilson, M. T., Uematsu, S., & Lesser, R. P. (1998). Functional mapping of human sensorimotor cortex with

- electrocorticographic spectral analysis. I. Alpha and beta event-related desynchronization. *Brain*, 121 ( Pt 12), 2271-2299. doi:10.1093/brain/121.12.2271
- Csicsvari, J., Jamieson, B., Wise, K. D., & Buzsaki, G. (2003). Mechanisms of gamma oscillations in the hippocampus of the behaving rat. *Neuron*, 37(2), 311-322.
- Dale, A. M., Fischl, B., & Sereno, M. I. (1999). Cortical surface-based analysis. I. Segmentation and surface reconstruction. *Neuroimage*, 9(2), 179-194. doi:10.1006/nimg.1998.0395
- de Hemptinne, C., Ryapolova-Webb, E. S., Air, E. L., Garcia, P. A., Miller, K. J., Ojemann, J. G., . . . Starr, P. A. (2013). Exaggerated phase-amplitude coupling in the primary motor cortex in Parkinson disease. *Proc Natl Acad Sci U S A*, 110(12), 4780-4785. doi:10.1073/pnas.1214546110
- de Hemptinne, C., Swann, N. C., Ostrem, J. L., Ryapolova-Webb, E. S., San Luciano, M., Galifianakis, N. B., & Starr, P. A. (2015). Therapeutic deep brain stimulation reduces cortical phase-amplitude coupling in Parkinson's disease. *Nat Neurosci*, 18(5), 779-786. doi:10.1038/nn.3997
- Degos, B., Deniau, J. M., Le Cam, J., Mailly, P., & Maurice, N. (2008). Evidence for a direct subthalamo-cortical loop circuit in the rat. *Eur J Neurosci*, 27(10), 2599-2610. doi:10.1111/j.1460-9568.2008.06229.x
- DeLong, M. R., & Wichmann, T. (2015). Basal Ganglia Circuits as Targets for Neuromodulation in Parkinson Disease. *JAMA Neurol*, 72(11), 1354-1360. doi:10.1001/jamaneurol.2015.2397
- Desikan, R. S., Segonne, F., Fischl, B., Quinn, B. T., Dickerson, B. C., Blacker, D., . . . Killiany, R. J. (2006). An automated labeling system for subdividing the human cerebral cortex on MRI scans into gyral based regions of interest. *Neuroimage*, 31(3), 968-980. doi:10.1016/j.neuroimage.2006.01.021



- Doyle, L. M., Yarrow, K., & Brown, P. (2005). Lateralization of event-related beta desynchronization in the EEG during pre-cued reaction time tasks. *Clin Neurophysiol*, *116*(8), 1879-1888. doi:10.1016/j.clinph.2005.03.017
- Duncan, J., & Owen, A. M. (2000). Common regions of the human frontal lobe recruited by diverse cognitive demands. *Trends in Neurosciences*, *23*(10), 475-483. doi:10.1016/s0166-2236(00)01633-7
- Engel, A. K., & Fries, P. (2010). Beta-band oscillations--signalling the status quo? *Curr Opin Neurobiol*, *20*(2), 156-165. doi:10.1016/j.conb.2010.02.015
- Enrici, I., Adenzato, M., Ardito, R. B., Mitkova, A., Cavallo, M., Zibetti, M., . . . Castelli, L. (2015). Emotion processing in Parkinson's disease: a three-level study on recognition, representation, and regulation. *PLoS One*, *10*(6), e0131470. doi:10.1371/journal.pone.0131470
- Fischl, B., Salat, D. H., Busa, E., Albert, M., Dieterich, M., Haselgrove, C., . . . Dale, A. M. (2002). Whole brain segmentation: automated labeling of neuroanatomical structures in the human brain. *Neuron*, *33*(3), 341-355. doi:10.1016/s0896-6273(02)00569-x
- Frank, M. J., Samanta, J., Moustafa, A. A., & Sherman, S. J. (2007). Hold your horses: impulsivity, deep brain stimulation, and medication in parkinsonism. *Science*, *318*(5854), 1309-1312. doi:10.1126/science.1146157
- Fries, P. (2005). A mechanism for cognitive dynamics: neuronal communication through neuronal coherence. *Trends Cogn Sci*, *9*(10), 474-480. doi:10.1016/j.tics.2005.08.011
- Fries, P. (2015). Rhythms for Cognition: Communication through Coherence. *Neuron*, *88*(1), 220-235. doi:10.1016/j.neuron.2015.09.034
- Fusar-Poli, P., Placentino, A., Carletti, F., Allen, P., Landi, P., Abbamonte, M., . . . Politi, P. L. (2009). Laterality effect on emotional faces processing: ALE meta-analysis of evidence. *Neurosci Lett*, *452*(3), 262-267. doi:10.1016/j.neulet.2009.01.065

- Gao, R., Peterson, E. J., & Voytek, B. (2017). Inferring synaptic excitation/inhibition balance from field potentials. *Neuroimage*, 158, 70-78. doi:10.1016/j.neuroimage.2017.06.078
- Gauggel, S., Rieger, M., & Feghoff, T. A. (2004). Inhibition of ongoing responses in patients with Parkinson's disease. *J Neurol Neurosurg Psychiatry*, 75(4), 539-544.  
doi:10.1136/jnnp.2003.016469
- Gold, A. L., Morey, R. A., & McCarthy, G. (2015). Amygdala-prefrontal cortex functional connectivity during threat-induced anxiety and goal distraction. *Biol Psychiatry*, 77(4), 394-403. doi:10.1016/j.biopsych.2014.03.030
- Gradinaru, V., Mogri, M., Thompson, K. R., Henderson, J. M., & Deisseroth, K. (2009). Optical deconstruction of parkinsonian neural circuitry. *Science*, 324(5925), 354-359.  
doi:10.1126/science.1167093
- Gunaydin, L. A., & Kreitzer, A. C. (2016). Cortico-Basal Ganglia Circuit Function in Psychiatric Disease. *Annu Rev Physiol*, 78, 327-350. doi:10.1146/annurev-physiol-021115-105355
- Hamilton, L. S., Chang, D. L., Lee, M. B., & Chang, E. F. (2017). Semi-automated Anatomical Labeling and Inter-subject Warping of High-Density Intracranial Recording Electrodes in Electrocorticography. *Front Neuroinform*, 11, 62. doi:10.3389/fninf.2017.00062
- Hammond, C., Bergman, H., & Brown, P. (2007). Pathological synchronization in Parkinson's disease: networks, models and treatments. *Trends Neurosci*, 30(7), 357-364.  
doi:10.1016/j.tins.2007.05.004
- Hannah, R., Muralidharan, V., Sundby, K. K., & Aron, A. R. (2019). Temporally-precise disruption of prefrontal cortex informed by the timing of beta bursts impairs human action-stopping. *bioRxiv*. doi:10.1101/843557
- Hariri, A. R., Bookheimer, S. Y., & Mazziotta, J. C. (2000). Modulating emotional responses: effects of a neocortical network on the limbic system. *Neuroreport*, 11(1), 43-48.
- Haynes, W. I., & Haber, S. N. (2013). The organization of prefrontal-subthalamic inputs in primates provides an anatomical substrate for both functional specificity and integration:

- implications for Basal Ganglia models and deep brain stimulation. *J Neurosci*, 33(11), 4804-4814. doi:10.1523/JNEUROSCI.4674-12.2013
- Herrick, I. A., Craen, R. A., Gelb, A. W., McLachlan, R. S., Girvin, J. P., Parrent, A. G., . . . Kirkby, J. (1997). Propofol sedation during awake craniotomy for seizures: electrocorticographic and epileptogenic effects. *Anesth Analg*, 84(6), 1280-1284.
- Herz, D. M., Tan, H., Brittain, J. S., Fischer, P., Cheeran, B., Green, A. L., . . . Brown, P. (2017). Distinct mechanisms mediate speed-accuracy adjustments in cortico-subthalamic networks. *Elife*, 6. doi:10.7554/eLife.21481
- Ibarretxe-Bilbao, N., Junque, C., Tolosa, E., Marti, M. J., Valldeoriola, F., Bargallo, N., & Zarei, M. (2009). Neuroanatomical correlates of impaired decision-making and facial emotion recognition in early Parkinson's disease. *Eur J Neurosci*, 30(6), 1162-1171. doi:10.1111/j.1460-9568.2009.06892.x
- Jackson, A., & Crossman, A. R. (1981). Subthalamic nucleus efferent projection to the cerebral cortex. *Neuroscience*, 6(11), 2367-2377. doi:10.1016/0306-4522(81)90023-3
- Jahanshahi, M., Obeso, I., Baunez, C., Alegre, M., & Krack, P. (2015). Parkinson's disease, the subthalamic nucleus, inhibition, and impulsivity. *Mov Disord*, 30(2), 128-140. doi:10.1002/mds.26049
- Jankovic, J. (2008). Parkinson's disease: clinical features and diagnosis. *J Neurol Neurosurg Psychiatry*, 79(4), 368-376. doi:10.1136/jnnp.2007.131045
- Kalia, L. V., & Lang, A. E. (2015). Parkinson's disease. *The Lancet*, 386(9996), 896-912. doi:10.1016/s0140-6736(14)61393-3
- Kelley, R., Flouty, O., Emmons, E. B., Kim, Y., Kingyon, J., Wessel, J. R., . . . Narayanan, N. S. (2018). A human prefrontal-subthalamic circuit for cognitive control. *Brain*, 141(1), 205-216. doi:10.1093/brain/awx300
- Kim, Y. C., Han, S. W., Alberico, S. L., Ruggiero, R. N., De Corte, B., Chen, K. H., & Narayanan, N. S. (2017). Optogenetic Stimulation of Frontal D1 Neurons Compensates

- for Impaired Temporal Control of Action in Dopamine-Depleted Mice. *Curr Biol*, 27(1), 39-47. doi:10.1016/j.cub.2016.11.029
- Kita, H., & Kitai, S. T. (1987). Efferent projections of the subthalamic nucleus in the rat: light and electron microscopic analysis with the PHA-L method. *J Comp Neurol*, 260(3), 435-452. doi:10.1002/cne.902600309
- Kita, T., & Kita, H. (2012). The subthalamic nucleus is one of multiple innervation sites for long-range corticofugal axons: a single-axon tracing study in the rat. *J Neurosci*, 32(17), 5990-5999. doi:10.1523/JNEUROSCI.5717-11.2012
- Kubaneck, J., & Schalk, G. (2015). NeuralAct: A Tool to Visualize Electrocortical (ECoG) Activity on a Three-Dimensional Model of the Cortex. *Neuroinformatics*, 13(2), 167-174. doi:10.1007/s12021-014-9252-3
- Kuhn, A. A., Williams, D., Kupsch, A., Limousin, P., Hariz, M., Schneider, G. H., . . . Brown, P. (2004). Event-related beta desynchronization in human subthalamic nucleus correlates with motor performance. *Brain*, 127(Pt 4), 735-746.
- Litvak, V., Jha, A., Eusebio, A., Oostenveld, R., Foltynie, T., Limousin, P., . . . Brown, P. (2011). Resting oscillatory cortico-subthalamic connectivity in patients with Parkinson's disease. *Brain*, 134(Pt 2), 359-374. doi:10.1093/brain/awq332
- Llinas, R. R. (1988). The intrinsic electrophysiological properties of mammalian neurons: insights into central nervous system function. *Science*, 242(4886), 1654-1664.
- Logothetis, N. K., Pauls, J., Augath, M., Trinath, T., & Oeltermann, A. (2001). Neurophysiological investigation of the basis of the fMRI signal. *Nature*, 412(6843), 150-157. doi:10.1038/35084005
- Lohani, S., Martig, A. K., Deisseroth, K., Witten, I. B., & Moghaddam, B. (2019). Dopamine Modulation of Prefrontal Cortex Activity Is Manifold and Operates at Multiple Temporal and Spatial Scales. *Cell Rep*, 27(1), 99-114 e116. doi:10.1016/j.celrep.2019.03.012

- Lombardi, W. J., Woolston, D. J., Roberts, J. W., & Gross, R. E. (2001). Cognitive deficits in patients with essential tremor. *Neurology*, *57*(5), 785-790. doi:10.1212/wnl.57.5.785
- Lopez-Azcarate, J., Tainta, M., Rodriguez-Oroz, M. C., Valencia, M., Gonzalez, R., Guridi, J., . . . Alegre, M. (2010). Coupling between beta and high-frequency activity in the human subthalamic nucleus may be a pathophysiological mechanism in Parkinson's disease. *J Neurosci*, *30*(19), 6667-6677. doi:10.1523/JNEUROSCI.5459-09.2010
- Malekmohammadi, M., Shahriari, Y., AuYong, N., O'Keefe, A., Bordelon, Y., Hu, X., & Pouratian, N. (2018). Pallidal stimulation in Parkinson disease differentially modulates local and network beta activity. *J Neural Eng*, *15*(5), 056016. doi:10.1088/1741-2552/aad0fb
- Manning, J. R., Jacobs, J., Fried, I., & Kahana, M. J. (2009). Broadband shifts in local field potential power spectra are correlated with single-neuron spiking in humans. *J Neurosci*, *29*(43), 13613-13620.
- Miocinovic, S., de Hemptinne, C., Chen, W., Isbaine, F., Willie, J. T., Ostrem, J. L., & Starr, P. A. (2018). Cortical Potentials Evoked by Subthalamic Stimulation Demonstrate a Short Latency Hyperdirect Pathway in Humans. *J Neurosci*, *38*(43), 9129-9141. doi:10.1523/JNEUROSCI.1327-18.2018
- Monakow, K. H.-v., Akert, K., & Kunzle, H. (1978). Projections of the precentral motor cortex and other cortical areas of the frontal lobe to the subthalamic nucleus in the monkey. *Experimental Brain Research*, *33*(3-4). doi:10.1007/bf00235561
- Montgomery, K. J., & Haxby, J. V. (2008). Mirror neuron system differentially activated by facial expressions and social hand gestures: a functional magnetic resonance imaging study. *J Cogn Neurosci*, *20*(10), 1866-1877. doi:10.1162/jocn.2008.20127
- Moonen, A. J. H., Weiss, P. H., Wiesing, M., Weidner, R., Fink, G. R., Reijnders, J., . . . Leentjens, A. F. G. (2017). An fMRI study into emotional processing in Parkinson's

- disease: Does increased medial prefrontal activation compensate for striatal dysfunction? *PLoS One*, 12(5), e0177085. doi:10.1371/journal.pone.0177085
- Mukamel, R., Gelbard, H., Arieli, A., Hasson, U., Fried, I., & Malach, R. (2005). Coupling between neuronal firing, field potentials, and fMRI in human auditory cortex. *Science*, 309(5736), 951-954. doi:10.1126/science.1110913
- Nambu, A., Takada, M., Inase, M., & Tokuno, H. (1996). Dual somatotopic representations in the primate subthalamic nucleus: evidence for ordered but reversed body-map transformations from the primary motor cortex and the supplementary motor area. *The Journal of Neuroscience*, 16(8), 2671-2683. doi:10.1523/jneurosci.16-08-02671.1996
- Nambu, A., Tokuno, H., Inase, M., & Takada, M. (1997). Corticosubthalamic input zones from forelimb representations of the dorsal and ventral divisions of the premotor cortex in the macaque monkey: comparison with the input zones from the primary motor cortex and the supplementary motor area. *Neuroscience Letters*, 239(1), 13-16. doi:10.1016/s0304-3940(97)00877-x
- Nambu, A., Tokuno, H., & Takada, M. (2002). Functional significance of the cortico–subthalamo–pallidal ‘hyperdirect’ pathway. *Neuroscience Research*, 43(2), 111-117. doi:10.1016/s0168-0102(02)00027-5
- Obeso, I., Wilkinson, L., & Jahanshahi, M. (2011). Levodopa medication does not influence motor inhibition or conflict resolution in a conditional stop-signal task in Parkinson's disease. *Exp Brain Res*, 213(4), 435-445. doi:10.1007/s00221-011-2793-x
- Ohara, S. (2000). Movement-related change of electrocorticographic activity in human supplementary motor area proper. *Brain*, 123(6), 1203-1215. doi:10.1093/brain/123.6.1203
- Panov, F., Levin, E., de Hemptinne, C., Swann, N. C., Qasim, S., Miocinovic, S., . . . Starr, P. A. (2017). Intraoperative electrocorticography for physiological research in movement

- disorders: principles and experience in 200 cases. *J Neurosurg*, 126(1), 122-131.  
doi:10.3171/2015.11.JNS151341
- Parker, K. L., Chen, K. H., Kingyon, J. R., Cavanagh, J. F., & Narayanan, N. S. (2015). Medial frontal approximately 4-Hz activity in humans and rodents is attenuated in PD patients and in rodents with cortical dopamine depletion. *J Neurophysiol*, 114(2), 1310-1320.  
doi:10.1152/jn.00412.2015
- Pasquereau, B., & Turner, R. S. (2017). A selective role for ventromedial subthalamic nucleus in inhibitory control. *Elife*, 6. doi:10.7554/eLife.31627
- Pesaran, B., Vinck, M., Einevoll, G. T., Sirota, A., Fries, P., Siegel, M., . . . Srinivasan, R. (2018). Investigating large-scale brain dynamics using field potential recordings: analysis and interpretation. *Nat Neurosci*, 21(7), 903-919. doi:10.1038/s41593-018-0171-8
- Phan, K. L., Wager, T., Taylor, S. F., & Liberzon, I. (2002). Functional neuroanatomy of emotion: a meta-analysis of emotion activation studies in PET and fMRI. *Neuroimage*, 16(2), 331-348. doi:10.1006/nimg.2002.1087
- Phillips, M. L., Drevets, W. C., Rauch, S. L., & Lane, R. (2003). Neurobiology of emotion perception I: the neural basis of normal emotion perception. *Biological Psychiatry*, 54(5), 504-514. doi:10.1016/s0006-3223(03)00168-9
- Ray, N. J., Brittain, J. S., Holland, P., Joundi, R. A., Stein, J. F., Aziz, T. Z., & Jenkinson, N. (2012). The role of the subthalamic nucleus in response inhibition: evidence from local field potential recordings in the human subthalamic nucleus. *Neuroimage*, 60(1), 271-278. doi:10.1016/j.neuroimage.2011.12.035
- Raz, A., Eimerl, D., Zaidel, A., Bergman, H., & Israel, Z. (2010). Propofol decreases neuronal population spiking activity in the subthalamic nucleus of Parkinsonian patients. *Anesth Analg*, 111(5), 1285-1289. doi:10.1213/ANE.0b013e3181f565f2
- Rolls, E. T. (2004). The functions of the orbitofrontal cortex. *Brain and Cognition*, 55(1), 11-29.  
doi:10.1016/s0278-2626(03)00277-x

- Schapira, A. H. V., Chaudhuri, K. R., & Jenner, P. (2017). Non-motor features of Parkinson disease. *Nat Rev Neurosci*, *18*(7), 435-450. doi:10.1038/nrn.2017.62
- Shin, H., Law, R., Tsutsui, S., Moore, C. I., & Jones, S. R. (2017). The rate of transient beta frequency events predicts behavior across tasks and species. *Elife*, *6*. doi:10.7554/eLife.29086
- Silberstein, P., Pogosyan, A., Kuhn, A. A., Hotton, G., Tisch, S., Kupsch, A., . . . Brown, P. (2005). Cortico-cortical coupling in Parkinson's disease and its modulation by therapy. *Brain*, *128*(Pt 6), 1277-1291. doi:10.1093/brain/awh480
- Singh, A., Richardson, S. P., Narayanan, N., & Cavanagh, J. F. (2018). Mid-frontal theta activity is diminished during cognitive control in Parkinson's disease. *Neuropsychologia*, *117*, 113-122. doi:10.1016/j.neuropsychologia.2018.05.020
- Sochurkova, D., & Rektor, I. (2003). Event-related desynchronization/synchronization in the putamen. An SEEG case study. *Exp Brain Res*, *149*(3), 401-404. doi:10.1007/s00221-003-1371-2
- Starr, P. A. (2002). Placement of deep brain stimulators into the subthalamic nucleus or Globus pallidus internus: technical approach. *Stereotact Funct Neurosurg*, *79*(3-4), 118-145. doi:10.1159/000070828
- Swann, N., Tandon, N., Canolty, R., Ellmore, T. M., McEvoy, L. K., Dreyer, S., . . . Aron, A. R. (2009). Intracranial EEG reveals a time- and frequency-specific role for the right inferior frontal gyrus and primary motor cortex in stopping initiated responses. *J Neurosci*, *29*(40), 12675-12685. doi:10.1523/JNEUROSCI.3359-09.2009
- Swann, N. C., Cai, W., Conner, C. R., Pieters, T. A., Claffey, M. P., George, J. S., . . . Tandon, N. (2012). Roles for the pre-supplementary motor area and the right inferior frontal gyrus in stopping action: electrophysiological responses and functional and structural connectivity. *Neuroimage*, *59*(3), 2860-2870. doi:10.1016/j.neuroimage.2011.09.049



- van Wijk, B. C., Beek, P. J., & Daffertshofer, A. (2012). Neural synchrony within the motor system: what have we learned so far? *Front Hum Neurosci*, *6*, 252.  
doi:10.3389/fnhum.2012.00252
- Verbruggen, F., Aron, A. R., Band, G. P., Beste, C., Bissett, P. G., Brockett, A. T., . . . Boehler, C. N. (2019). A consensus guide to capturing the ability to inhibit actions and impulsive behaviors in the stop-signal task. *Elife*, *8*. doi:10.7554/eLife.46323
- Wagenbreth, C., Wattenberg, L., Heinze, H. J., & Zaehle, T. (2016). Implicit and explicit processing of emotional facial expressions in Parkinson's disease. *Behav Brain Res*, *303*, 182-190. doi:10.1016/j.bbr.2016.01.059
- Walker, H. C., Huang, H., Gonzalez, C. L., Bryant, J. E., Killen, J., Cutter, G. R., . . . Watts, R. L. (2012). Short latency activation of cortex during clinically effective subthalamic deep brain stimulation for Parkinson's disease. *Mov Disord*, *27*(7), 864-873.  
doi:10.1002/mds.25025
- Wang, D. D., de Hemptinne, C., Miocinovic, S., Ostrem, J. L., Galifianakis, N. B., San Luciano, M., & Starr, P. A. (2018). Pallidal Deep-Brain Stimulation Disrupts Pallidal Beta Oscillations and Coherence with Primary Motor Cortex in Parkinson's Disease. *J Neurosci*, *38*(19), 4556-4568. doi:10.1523/JNEUROSCI.0431-18.2018
- Wang, S., Yu, R., Tyszka, J. M., Zhen, S., Kovach, C., Sun, S., . . . Rutishauser, U. (2017). The human amygdala parametrically encodes the intensity of specific facial emotions and their categorical ambiguity. *Nat Commun*, *8*, 14821. doi:10.1038/ncomms14821
- Wessel, J. R., & Aron, A. R. (2013). Unexpected events induce motor slowing via a brain mechanism for action-stopping with global suppressive effects. *J Neurosci*, *33*(47), 18481-18491. doi:10.1523/JNEUROSCI.3456-13.2013
- Widge, A. S., Zorowitz, S., Basu, I., Paulk, A. C., Cash, S. S., Eskandar, E. N., . . . Dougherty, D. D. (2019). Deep brain stimulation of the internal capsule enhances human cognitive control and prefrontal cortex function. *Nat Commun*, *10*(1), 1536.

- Wieser, M. J., Muhlberger, A., Alpers, G. W., Macht, M., Ellgring, H., & Pauli, P. (2006). Emotion processing in Parkinson's disease: dissociation between early neuronal processing and explicit ratings. *Clin Neurophysiol*, *117*(1), 94-102. doi:10.1016/j.clinph.2005.09.009
- Zavala, B., Tan, H., Ashkan, K., Foltynie, T., Limousin, P., Zrinzo, L., . . . Brown, P. (2016). Human subthalamic nucleus-medial frontal cortex theta phase coherence is involved in conflict and error related cortical monitoring. *Neuroimage*, *137*, 178-187. doi:10.1016/j.neuroimage.2016.05.031
- Zavala, B. A., Tan, H., Little, S., Ashkan, K., Hariz, M., Foltynie, T., . . . Brown, P. (2014). Midline frontal cortex low-frequency activity drives subthalamic nucleus oscillations during conflict. *J Neurosci*, *34*(21), 7322-7333. doi:10.1523/JNEUROSCI.1169-14.2014

## Publishing Agreement

It is the policy of the University to encourage open access and broad distribution of all theses, dissertations, and manuscripts. The Graduate Division will facilitate the distribution of UCSF theses, dissertations, and manuscripts to the UCSF Library for open access and distribution. UCSF will make such theses, dissertations, and manuscripts accessible to the public and will take reasonable steps to preserve these works in perpetuity.

I hereby grant the non-exclusive, perpetual right to The Regents of the University of California to reproduce, publicly display, distribute, preserve, and publish copies of my thesis, dissertation, or manuscript in any form or media, now existing or later derived, including access online for teaching, research, and public service purposes.

DocuSigned by:

*Witney Chen*

AD4B649975A34FE...

\_\_\_\_\_  
Author Signature

1/28/2020

\_\_\_\_\_  
Date